



HAL
open science

The nitrogen cycles on Pluto over seasonal and astronomical timescales

T. Bertrand, F. Forget, O.M. Umurhan, W.M. Grundy, B. Schmitt, S. Protopapa, A. M Zangari, O.L. White, P.M. Schenk, K. N Singer, et al.

► To cite this version:

T. Bertrand, F. Forget, O.M. Umurhan, W.M. Grundy, B. Schmitt, et al..
The nitrogen cycles on Pluto over seasonal and astronomical timescales. Icarus, 2018, 309, pp.277-296. 10.1016/j.icarus.2018.03.012 . hal-01744474

HAL Id: hal-01744474

<https://hal.sorbonne-universite.fr/hal-01744474>

Submitted on 27 Mar 2018

HAL is a multi-disciplinary open access archive for the deposit and dissemination of scientific research documents, whether they are published or not. The documents may come from teaching and research institutions in France or abroad, or from public or private research centers.

L'archive ouverte pluridisciplinaire **HAL**, est destinée au dépôt et à la diffusion de documents scientifiques de niveau recherche, publiés ou non, émanant des établissements d'enseignement et de recherche français ou étrangers, des laboratoires publics ou privés.

1 **The nitrogen cycles on Pluto over seasonal and**
2 **astronomical timescales**

3 T. Bertrand^{a,b}, F. Forget^a, O.M. Umurhan^b, W.M. Grundy^c,
4 B. Schmitt^d, S. Protopapa^{e,f}, A.M. Zangari^f, O.L. White^b,
5 P.M. Schenk^g, K.N. Singer^f, A. Stern^f, H.A. Weaver^h,
6 L.A. Young^f, K. Ennico^b, C.B. Olkin^f,
7 the New Horizons Science Team,

8 ^a*Laboratoire de Météorologie Dynamique, IPSL, Sorbonne Universités, UPMC Univ*
9 *Paris 06, CNRS, 4 place Jussieu, 75005 Paris, France.*

10 ^b*National Aeronautics and Space Administration (NASA), Ames Research Center,*
11 *Space Science Division, Moffett Field, CA 94035, United States*

12 ^c*Lowell Observatory, Flagstaff, AZ, United States*

13 ^d*Université Grenoble Alpes, CNRS, Institut de Planétologie et Astrophysique de*
14 *Grenoble, F-38000 Grenoble, France*

15 ^e*University of Maryland, Department of Astronomy, College Park, MD 20742,*
16 *United States*

17 ^f*Southwest Research Institute, Boulder, CO 80302, United States*

18 ^g*Lunar and Planetary Institute, 3600 Bay Area Blvd. Houston, TX 77058, United*
19 *States*

20 ^h*Johns Hopkins University Applied Physics Laboratory, Laurel, MD 20723, United*
21 *States*

22 Copyright © 2005, 2006 Ross A. Beyer, David P. O'Brien, Paul Withers, and Gwen Bart

23 Number of pages: 49

24 Number of tables: 1

25 Number of figures: 16

26 **Proposed Running Head:**

27

28 **Please send Editorial Correspondence to:**

29

30 Tanguy Bertrand

31 Laboratoire de Météorologie Dynamique, CNRS/UPMC (France)

32

33 Email: tanguy.bertrand@lmd.jussieu.fr

34

35 **ABSTRACT**

36 Pluto's landscape is shaped by the endless condensation and sublimation cy-
37 cles of the volatile ices covering its surface. In particular, the Sputnik Planitia
38 ice sheet, which is thought to be the main reservoir of nitrogen ice, displays a
39 large diversity of terrains, with bright and dark plains, small pits and troughs,
40 topographic depressions and evidences of recent and past glacial flows. Outside
41 Sputnik Planitia, New Horizons also revealed numerous nitrogen ice deposits,
42 in the eastern side of Tombaugh Regio and at mid-northern latitudes.

43 These observations suggest a complex history involving volatile and glacial
44 processes occurring on different timescales. We present numerical simulations
45 of volatile transport on Pluto performed with a model designed to simulate
46 the nitrogen cycle over millions of years, taking into account the changes
47 of obliquity, solar longitude of perihelion and eccentricity as experienced by
48 Pluto. Using this model, we first explore how the volatile and glacial activity
49 of nitrogen within Sputnik Planitia has been impacted by the diurnal, seasonal
50 and astronomical cycles of Pluto. Results show that the obliquity dominates
51 the N_2 cycle and that over one obliquity cycle, the latitudes of Sputnik Planitia
52 between 25°S - 30°N are dominated by N_2 condensation, while the northern
53 regions between 30°N - 50°N are dominated by N_2 sublimation. We find that
54 a net amount of 1 km of ice has sublimed at the northern edge of Sputnik
55 Planitia during the last 2 millions of years. It must have been compensated
56 by a viscous flow of the thick ice sheet. By comparing these results with
57 the observed geology of Sputnik Planitia, we can relate the formation of the
58 small pits and the brightness of the ice at the center of Sputnik Planitia to
59 the sublimation and condensation of ice occurring at the annual timescale,
60 while the glacial flows at its eastern edge and the erosion of the water ice
61 mountains all around the ice sheet are instead related to the astronomical
62 timescale. We also perform simulations including a glacial flow scheme which
63 shows that the Sputnik Planitia ice sheet is currently at its minimum extent
64 at the northern and southern edges. We also explore the stability of N_2 ice
65 deposits outside the latitudes and longitudes of the Sputnik Planitia basin.
66 Results show that N_2 ice is not stable at the poles but rather in the equatorial
67 regions, in particular in depressions, where thick deposits may persist over tens
68 of millions of years, before being trapped in Sputnik Planitia. Finally, another
69 key result is that the minimum and maximum surface pressures obtained over
70 the simulated millions of years remain in the range of milli-Pascals and Pascals,
71 respectively. This suggests that Pluto never encountered conditions allowing
72 liquid nitrogen to flow directly on its surface. Instead, we suggest that the
73 numerous geomorphological evidences of past liquid flow observed on Pluto's
74 surface are the result of liquid nitrogen that flowed at the base of thick ancient
75 nitrogen glaciers, which have since disappeared.

76 *Keywords:* Pluto; nitrogen; paleo; Modelling; GCM; Sputnik Planitia;

⁷⁷ <http://icarus.cornell.edu/information/keywords.html>

78 1 Introduction

79 1.1 Pluto's ices observations

80 Among the most striking observations of Pluto made by New Horizons in July
81 2015 is the prominent nitrogen ice sheet laying in Sputnik Planitia^{*} (SP),
82 which displays a highly diverse range of terrains, as described by [White et al.](#)
83 (2017); [Moore et al.](#) (2017); [McKinnon et al.](#) (2016). First, bright nitrogen-
84 rich plains (0°-30°N) contrast with darker plains at higher latitudes (30°-40°N)
85 having higher amounts of diluted methane, and even darker, more methane
86 and tholins rich plains (40°-50°N) at the northern edge of SP (see composition
87 maps Fig. 5.C in [Protopapa et al.](#) (2017) and Figs. 13.2, 15 and 18 in [Schmitt](#)
88 [et al.](#) (2017)). Cellular patterns, indicative of active solid-state convection
89 ([McKinnon et al., 2016](#); [Trowbridge et al., 2016](#)), are observed in the northern
90 part of SP (0°-40°N) but not in the southern part of SP (0°-25°S). The absence
91 of convection cells coincides with the presence of hundred meters deep pits
92 on the surface of the ice sheet ([Moore et al., 2017](#)). Glacial flow activity is
93 observed through the valleys at the eastern edge of SP (flowing toward the
94 center of SP from the uplands, 20°S-30°N) and at the northern edge of SP
95 (flowing outward the basin), as shown by [Howard et al.](#) (2017) and [Umurhan](#)
96 [et al.](#) (2017). Finally, rugged water ice mountains surround the SP region (Al-
97 Idrisi, Hillary and Tenzing Montes), suggesting that they have been eroded
98 and shaped over time by the action of glacial flow ([Stern et al., 2015](#); [Howard](#)
99 [et al., 2017](#)), as the terrestrial “Nunataks” in Greenland and Antarctica.

100 New Horizons also revealed bright deposits of nitrogen outside SP. In the
101 equatorial regions, the eastern side of Tombaugh Regio is covered by numerous
102 patches of nitrogen ice, which are also observed further east in the depressions
103 and valleys between the high altitude “bladed terrains” deposits ([Moore et al.,](#)
104 [2017](#)) and further west at the bottom of deep craters ([Schmitt et al., 2017](#)).
105 In addition, bright patches of nitrogen ice are detected over a latitudinal band
106 between 30°N and 60°N ([Schmitt et al., 2017](#)).

107 What is the history of Sputnik Planitia and the nitrogen deposits? Resurfacing
108 by glacial flow, solid-state convection, or nitrogen sublimation and condensa-
109 tion have been proposed to explain the formation and disappearance of the
110 pits and polygonal cells within SP ([White et al., 2017](#); [Moore et al., 2017](#)).
111 In addition, sublimation-condensation processes are thought to drive the dif-
112 ference in ice albedos, composition and distribution outside Sputnik Planitia
113 ([White et al., 2017](#); [Protopapa et al., 2017](#); [Howard et al., 2017](#)). However,
114 the timescales and amounts of ice involved are not known, which prevents us

* The place names mentioned in this paper include a mix of officially approved names and informal names.

115 from distinguishing the roles of each process and the nature of the reservoirs
116 (perennial/seasonal).

117 *1.2 Modelling of the present-day Pluto's volatile cycle*

118 The condensation and sublimation of Pluto's volatiles and their transport
119 over several Pluto seasons has been modelled under current orbital conditions
120 by [Bertrand and Forget \(2016\)](#), that is with an obliquity of 119.6° , an orbit
121 eccentricity of 0.2488 and a solar longitude at perihelion of 3.8° . Solar lon-
122 gitude at perihelion ($L_{s \text{ peri}}$) is the Pluto-Sun angle at perihelion, measured
123 from the Northern Hemisphere spring equinox ($L_{s \text{ peri}}=0^\circ$ when the perihe-
124 lion coincides with the northern spring equinox). It defines the link between
125 Pluto season and the distance from the Sun (and thus also the duration of the
126 season). Results using a seasonal thermal inertia for the sub-surface within
127 $500\text{-}1500 \text{ J s}^{-1/2} \text{ m}^{-2} \text{ K}^{-1}$ showed that nitrogen and carbon monoxide (CO)
128 are trapped inside the Sputnik Planitia basin because its low altitude (its sur-
129 face is located at $\sim 3 \text{ km}$ below the surroundings terrains) induces a higher
130 condensation temperature of the ice (compared to the ice outside the basin),
131 leading to an enhanced thermal infrared cooling and condensation rate at the
132 bottom of the basin ([Bertrand and Forget, 2016](#)). Note that the reverse oc-
133 curs on Earth, where the ice caps form at the poles and at high altitude. In
134 these simulations, methane also accumulates in SP but its low volatility allows
135 it to condense on warmer surfaces (where N_2 and CO would instantly subli-
136 mate) and form seasonal frosts of pure methane everywhere in the fall-winter
137 hemisphere except at the equator which tends to remain free of volatile ice.
138 Results also showed that bright methane frosts in the northern hemisphere
139 could favour nitrogen condensation on it and thus lead to the formation of
140 a seasonal nitrogen polar cap. These polar deposits sublime in spring from
141 the pole and in 2015, only a latitudinal band of nitrogen frost around 45°N
142 remained.

143 *1.3 The changes of obliquity and orbital parameters over astronomical timescales*

144 While [Bertrand and Forget \(2016\)](#) focused on the volatile cycles in Pluto's
145 current orbital conditions, these latter are known to vary over timescales of
146 100 000 terrestrial years. Pluto's high obliquity varies between 104° and 127°
147 over 2.8 Myrs. The solar longitude of perihelion of Pluto's orbit varies with a
148 precession period of 3.7 Myrs, while its eccentricity oscillates between 0.222
149 and 0.266 with a 3.95 Myrs period ([Earle et al., 2017](#); [Binzel et al., 2017](#);
150 [Hamilton et al., 2016](#)). The variation of these parameters, known as the Mi-
151 lankovitch mechanism, also occurs on the Earth, Mars and Titan. The pa-

152 rameters combine to modulate the solar insolation and surface temperatures,
153 forcing the volatile ices that form glaciers, frost or lakes to migrate in different
154 regions with time.

155 On Earth, obliquity changes are known to have played a critical role in pacing
156 glacial and interglacial eras. Because of the absence of a big moon and its
157 proximity to Jupiter, Mars has an obliquity which varies much more strongly
158 than on Earth, and experienced periods when poles were warmer than equator,
159 like on Pluto. Many surface structures of Mars are thought to be the effect
160 of orbital forcing or of the Milankovitch cycle on the climate of Mars. For
161 instance, climate modeling efforts showed that during high obliquity periods,
162 ice can be deposited almost anywhere in the mid-latitudes, explaining the
163 evidences of glaciers and widespread ground-ice mantle in these regions, while
164 during low obliquity ice is transported back to the poles (Levrard et al., 2007;
165 Mischna et al., 2003; Forget et al., 2006; Madeleine et al., 2009, e.g.). On
166 Titan, the cooler summers in the north pole explain the lakes preference for
167 the northern latitudes (Schneider et al., 2012). The differing solar insolation
168 between both hemisphere would result from the eccentricity of Titans orbit
169 and the obliquity of Saturn, coupled with Titans low inclination and obliquity
170 (Aharonson et al., 2009). Climatic changes similar in scale to Earths climatic
171 cycles are expected as the obliquity and orbital parameters of Titan vary on
172 timescales of tens of thousands of years.

173 By comparison with the Earth, Mars and Titan, Pluto’s climate is expected
174 to be dictated by the universal Milankovitch mechanism as well. A few studies
175 have explored the variation of insolation on Pluto caused by the changes of
176 obliquity, solar longitude of perihelion and eccentricity, and have shown that
177 the obliquity is the main driver of Pluto’s insolation (Earle et al., 2017; Binzel
178 et al., 2017; Stern et al., 2017). However these thermal models neglected the
179 impact of seasonal thermal inertia (TI), which strongly controls surface tem-
180 peratures (see Section 3) and they did not address the transport of volatiles,
181 necessary to fully understand how Pluto’s ices evolved in the past.

182 *1.4 Objectives of this paper*

183 Our objective is to investigate the evolution and distribution of nitrogen ice on
184 Pluto over the past millions of Earth years (Myrs). To do that, we extend the
185 Bertrand and Forget (2016) study and use the Pluto’s volatile transport model,
186 taking into account (1) the changes of the astronomical cycles (obliquity, so-
187 lar longitude of perihelion and eccentricity) induced by the perturbation of
188 the Sun on the Pluto-Charon binary system (Dobrovolskis et al., 1997), (2)
189 realistic reservoirs of nitrogen ice, (3) the changes of ice thickness induced by
190 glacial flow.

191 Pluto’s astronomical cycles are thought to have been stable over at least the
192 last 20 million years [Binzel et al. \(2017\)](#), and probably even before. The first
193 reason is that Pluto’s orbit is in a relatively isolated region of the Solar System,
194 never getting within ~ 11 AU of any major planet, and it is therefore subject to
195 very little perturbations ([Dobrovolskis et al., 1997](#)). In addition, [Binzel et al.](#)
196 [\(2017\)](#) state that the presence of ancient craters at the equator demonstrates
197 a certain stability of the astronomical cycles, which could extend back in time
198 by hundreds of Myrs (otherwise the craters would have been eroded away
199 or completely buried). In this paper, we assume that the astronomical cycles
200 remained stable during the last 30 Myrs.

201 Here we explore the impact of orbital and obliquity changes on the nitrogen
202 cycle only. Thus, all the simulations of this paper are performed without the
203 cycles of methane and CO. This choice is driven by the fact that the number of
204 sensitivity parameters and initial states explored in this work already makes it
205 start at a certain complexity level. In fact, we know from [Bertrand and Forget](#)
206 [\(2016\)](#) that CO “follows“ N₂ and remains always trapped in N₂ ice. The case
207 of CH₄ ice is much more complex because it can form CH₄-rich deposits (with
208 3-5% N₂) on Pluto’s surface and trigger N₂ condensation if its albedo is high
209 enough. Exploring the cycle of methane over astronomical timescales and its
210 impact on Pluto’s climate will be the topic of a separate paper.

211 In Section 2, we describe the Pluto volatile transport model and its recent
212 development allowing for the simulations of the nitrogen cycle over several
213 astronomical cycles (in particular, the model includes an ice redistribution
214 algorithm, glacial flow modelling, changes of topography, obliquity, and orbital
215 parameters with time).

216 In Section 3, we show the impact of the obliquity, the orbital parameters and
217 the thermal inertia on the surface temperatures averaged over the past Myrs.

218 Then, in Section 4, we investigate how the past cycles of nitrogen sublimation
219 and condensation (at diurnal, seasonal, astronomical timescales), as well as
220 the glacial flow of N₂ ice may have shaped Sputnik Planitia as it is observed
221 today.

222 In Section 5, we explore possible steady state for nitrogen deposits outside
223 Sputnik Planitia, by performing simulations over the last 30 Myrs with differ-
224 ent reservoirs of N₂ ice initially placed at the poles, at the equator or uniformly
225 spread over the surface. We also explore the maximum and minimum surface
226 pressures Pluto encountered during that time. We discuss these results in Sec-
227 tion 6.

228 2 Model description

229 We use the latest version of the Pluto volatile transport model of the Labo-
230 ratoire de Météorologie Dynamique (LMD) (Bertrand and Forget, 2016, see
231 Methods).

232 This model represents the physical processes that control the condensation and
233 sublimation of Pluto’s volatiles (insolation, surface thermal balance) and uses
234 a simple global mixing function to parametrize the atmospheric transport and
235 dynamics. Note that in this model, the atmosphere is considered transparent:
236 there is no atmospheric process taken into account aside from the condensa-
237 tion, sublimation and exchanges of latent heat with the surface. Such a model
238 works well on Pluto because the surface energy balance is not significantly
239 sensitive to the atmospheric sensible heat flux and to the radiative transfer
240 through the air.

241 In this section, we describe the grid and surface properties used in our sim-
242 ulations (Sections 2.1 and 2.2) and the recent developments performed in
243 the code, allowing the simulation of the nitrogen cycles over astronomical
244 timescales. These improvements concern a paleoclimate mode (Section 2.3),
245 the implementation of the latest topography of Pluto with a specific relief for
246 the SP basin (Section 2.4) and a glacial flow scheme (Section 2.5). Note that
247 all figures and maps are shown using the IAU convention, spin north system
248 for definition of the north pole (Buie et al., 1997; Zangari, 2015), that is with
249 spring-summer in the northern hemisphere during the 21th Century.

250 2.1 Model grid

251 In this paper, the simulations investigating the stability of N₂ ice deposits
252 outside SP (Section 5) have been performed with a horizontal grid of 32×24
253 points, that is a grid-point spacing of 7.5° latitude by 11.25° longitude and
254 a spatial resolution of about 150 km. Simulations focusing on the N₂ cycle
255 within Sputnik Planitia (Section 4) have been performed with a twice higher
256 spatial resolution of 5.6° in longitude and 1.875° in latitude.

257 2.2 Model grid and surface properties

258 As in Bertrand and Forget (2016), the reference albedo of nitrogen ice is
259 set to 0.7, and its emissivity to 0.8. The albedo and emissivity of the bare
260 ground (free of N₂ ice) are set to 0.1 and 1 respectively. In the soil model, the
261 near-surface layers have a low-TI to capture the short-period diurnal thermal

262 waves, while the deeper layers have a high-TI to capture the much longer
 263 seasonal thermal waves. The diurnal TI is set to $20 \text{ J s}^{-1/2} \text{ m}^{-2}\text{K}^{-1}$ (or SI),
 264 as inferred from Spitzer thermal observations (Lellouch et al., 2011). In this
 265 paper, simulations have been performed without a diurnal cycle (the insolation
 266 is averaged over the Pluto day) and therefore the diurnal TI has no impact on
 267 the results. The reference seasonal thermal inertia TI is uniformly set to 800 SI,
 268 because it corresponds to the best case simulation reproducing the threefold
 269 increase of surface pressure observed between 1988 and 2015 (Bertrand and
 270 Forget, 2016) and the 1-1.2 Pa value in 2015. Here we assume that all terrains
 271 (water ice bedrock and nitrogen ice) have the same TI. In this paper, sensitivity
 272 simulations have also been performed using 400 and 1200 SI. The modelled
 273 diurnal and annual skin depths are 0.008 m and 20-60 m respectively.

274 To adequately resolve these scale lengths, the subsurface is divided into 24
 275 discrete layers, with a geometrically stretched distribution of layers with higher
 276 resolution near the surface to capture the short waves (the depth of the first
 277 layer is $z_1=1.4\times 10^{-4}\text{m}$) and a coarser grid for deeper layers and long waves
 278 (the deepest layer depth is near 1000 m). The depth of each layer is given by:

$$279 \quad z_k = z_1 2^{k-1} \quad (1)$$

280 Our simulations are performed assuming no internal heat flux. Adding an
 281 internal heat flux of few mW m^{-2} , as suggested in Robuchon and Nimmo
 282 (2011) for Pluto, does not change significantly the results. Our tests show
 283 that the surface temperature increases by 0.2 K when taking into account an
 284 internal heat flux of 3 mW m^{-2} (see the discussion in 2.5).

285 Note that the seasonal thermal inertia of N_2 ice does not impact the amount
 286 of condensed or sublimed N_2 ice to first order.

287 Indeed, as shown by equation 12 and 13 in Forget et al. (2017), the varia-
 288 tion of the exchanged mass between the surface and the atmosphere δm_0 is
 289 nearly proportional to a product involving the surface heat capacity c_s (in
 290 $\text{J m}^{-2} \text{ K}^{-1}$), which depends on the thermal inertia:

$$291 \quad \delta m_0 \propto \frac{c_s}{L_{\text{N}_2}} \Delta T_s \quad (2)$$

292 with L_{N_2} the latent heat of N_2 ($2.5 \cdot 10^5 \text{ J kg}^{-1}$) and T_s the surface temperature.
 293 Yet ΔT_s is nearly proportional to $\frac{F}{c_s}$ to first order, with F the thermal flux
 294 absorbed by the surface (W m^{-2}). Hence:

$$295 \quad \delta m_0 \propto \frac{F}{L_{\text{N}_2}} \quad (3)$$

296 Consequently, to first order, δm_0 is independent of c_s and of thermal inertia.

297 2.3 The paleoclimate mode and ice equilibration algorithm

298 Because the solar flux received by Pluto's surface is very low (about 1 W m^{-2}),
299 and because Pluto makes a full orbit around the Sun every 248 years, the
300 modelled surface and subsurface temperatures and the surface ice distribution
301 require simulations of several Pluto years to reach a steady state. Running the
302 Pluto volatile transport model with the N_2 cycle only can take around 5 min-
303 utes of computing time for one simulated Pluto year at the chosen resolution.
304 Consequently, running climate evolution over 1 Myrs would require 2 weeks
305 of simulation and performing paleoclimate simulations over several astronom-
306 ical cycles, e.g. over the last 30 Myrs, would be prohibitively time-consuming.
307 To resolve this problem, we implemented in the model a paleoclimate mode
308 containing an ice iteration scheme. The algorithm is similar to the approach
309 taken for Mars simulations in [Wordsworth et al. \(2013\)](#): Starting from the
310 initial surface ice distribution q^- (kg m^{-2}), the model is ran normally for 5
311 Pluto years (Step 1), in order to reach repeatable annual condensation and
312 sublimation rates as well as repeatable annual temperatures variations. In the
313 last year, the annual mean ice rate of change $\langle dq/dt \rangle$ is evaluated at each
314 grid point and then multiplied by a multiple-year timestep Δt to give the
315 updated surface ice distribution q^+ and reservoir (Step 2):

$$316 \quad q_{ice}^+ = q_{ice}^- + \left\langle \frac{dq_{ice}}{dt} \right\rangle \Delta t \quad (4)$$

317 If the reservoir of ice at one gridpoint has entirely sublimed during the paleo-
318 timestep Δt , the amount of ice is set to 0 kg m^{-2} , and after redistribution,
319 the amount in each cell is normalized to conserve the total nitrogen mass (ice
320 and vapour) in the system. Then, the topography is updated according to
321 the new thickness of the deposits on the surface (Step 3). Finally, the orbital
322 parameters and the obliquity are changed according to the new date of the
323 simulation (Step 4). Then the loop started again: the model is run again for 5
324 Pluto years ; at each paleo-timestep Δt , the topography is updated according
325 to the annual mean ice rate of the last Pluto year, and the orbital parameters
326 and the obliquity of Pluto are changed according to the new date $t+\Delta t$.

327 The paleo-timestep must be small enough so that the changes of obliquity and
328 orbital parameters allow the surface ice distribution to reach a steady state
329 at each paleo timestep, but it must be high enough to reduce significantly
330 the computing time of the simulation. In our simulations described here, we
331 typically used $\Delta t = 50\,000$ Earth years, which corresponds to about 200 Pluto
332 orbits and a maximal change in its obliquity of 1° of latitude ([Binzel et al.](#),

333 2017).

334 The changes of obliquity, solar longitude of perihelion and eccentricity are
335 taken from Earle et al. (2017) and Dobrovolskis et al. (1997) and are shown on
336 Figure 1. Assuming that the obliquity and orbital parameters remain periodic
337 with time, we extrapolated the data back to 30 Myrs ago, which corresponds
338 to the starting date of our simulations. Here the variations of eccentricity
339 (between $e_{min}=0.222$ and $e_{max}=0.266$) are taken into account but not shown
340 for the sake of simplicity. Note that its impact on Pluto’s climate is negligible
341 compared to the change of the two other parameters (Hamilton et al., 2016).

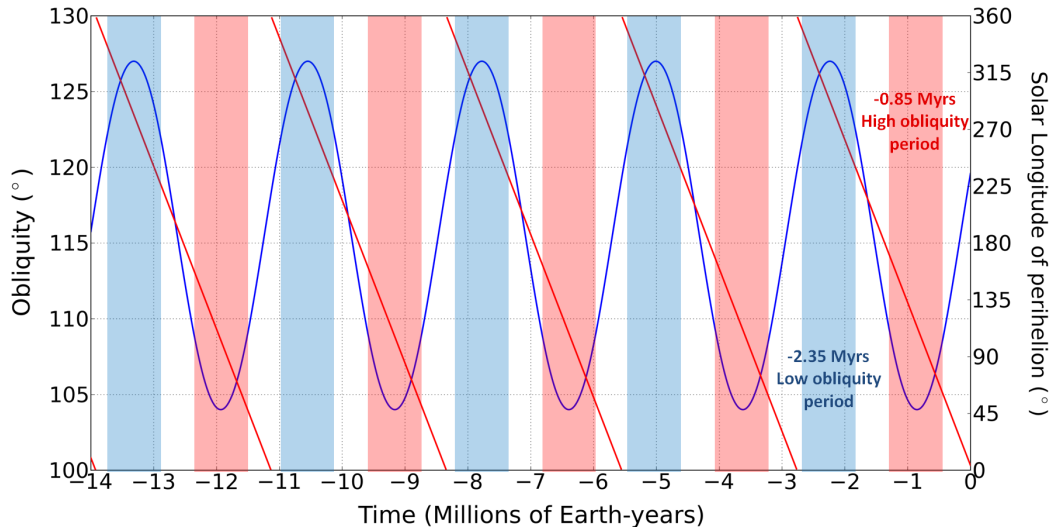


Fig. 1. The astronomical cycles of Pluto during the past 14 Earth million years (~ 5 obliquity cycles): cycles of obliquity (blue solid line, period: 2.8 Myrs) and $L_s\ peri$ (red solid line, period: 3.7 Myrs). High obliquity refers to values close to 90° , while "low" obliquity is used here to designate the periods with minimal obliquity, that is far from 90° , although here it remains relatively high compared to other bodies in the Solar System. Present-day Pluto (obliquity= 119.6° , that is 60.4° in retrograde rotation) is subject to an intermediate obliquity (white background). A low obliquity period occurred 2.35 Myrs ago (blue background) and a high obliquity period 0.9 Myrs ago (red background).

342 2.4 Topography

343 The simulations are performed with the latest topography data of Pluto
344 (Schenk et al., 2018a). In the south hemisphere, where there is no data, we
345 considered a flat surface (at mean radius). If we model a surface topography in
346 the southern hemisphere varying of few kilometers, results remain unchanged
347 and N_2 ice will accumulate at similar latitudes.

348 In the simulations performed with glacial flow of N₂ ice, we modified the
349 topography of Sputnik Planitia by placing the bedrock much deeper than the
350 actual surface of SP, in order to represent SP with realistic amounts of ice.
351 We assume that the bedrock below the center of SP is a 10 km deep elliptical
352 basin, which is in the range of the estimates for the thickness of volatiles
353 where polygonal cells are observed (Moore et al., 2016; McKinnon et al., 2016;
354 Trowbridge et al., 2016; Keane et al., 2016).

355 The elliptical basin covers the latitudes 10°S-50°N (Figure 2), with a semi
356 major axis of 1200 km and the foci F=(42°N,163°E) and F'=(1.75°N,177°W).
357 The edges and the southern parts of the basin are less deep, in accordance
358 with typical impact basin shapes and the absence of convective cells there. We
359 have different cases where we placed the bedrock in these areas at 4 km or
360 5 km below the mean surface level, as shown by Figure 2. In the simulations
361 focusing on N₂ ice inside SP (Section 4), this modelled basin is then filled
362 with N₂ ice up to 2.5 km below the mean surface level, which corresponds
363 to the observed altitude of the surface of the SP ice sheet (in that case, the
364 thickness of ice at the centre of SP would be 10-2.5=7.5 km). Note that in
365 the modeled topography we removed the water ice mountains from Al-Idrisi
366 to Hillary Montes for the sake of simplicity.

367 2.5 *Ice viscous flow modelling*

368 Despite being completely frozen, Plutos surface is remarkably active. Evidence
369 of current and past flowing nitrogen ice have been observed by New Horizons
370 all around Sputnik Planitia (rugged eroded water ice mountains, glaciers with
371 moraine-like ridges...) and at higher latitudes (Stern et al., 2017; Howard et al.,
372 2017; Umurhan et al., 2017).

373 In order to represent the nitrogen ice flow in the model, we use a laminar
374 glacial flow scheme, as presented in Umurhan et al. (2017), which is based on
375 the N₂ ice rheology for low surface temperatures described in Yamashita et al.
376 (2010) and depends on the thickness and temperature of the ice. The model
377 has several limitations. First, very little laboratory data is available under
378 Plutonian surface conditions and the rheology of solid N₂ has not been very
379 well constrained to date (see Umurhan et al. (2017)), not to mention the rhe-
380 ology of the possible ice mixtures on Pluto and of the α crystalline structure.
381 N₂ ice behaves as a viscous fluid with a viscosity ranging between 10⁸-10¹²
382 Pa s at stresses of 10⁵ Pa (Durham et al., 2010), and flows more rapidly than
383 water ice on Earth, despite the lower gravity of Pluto. Secondly, the model
384 strongly depends on the height of the column of ice, its temperature and the
385 N₂ ice rheology properties, which are poorly known (Umurhan et al., 2017).
386 In addition, we are limited by the horizontal resolution, which prevents us to

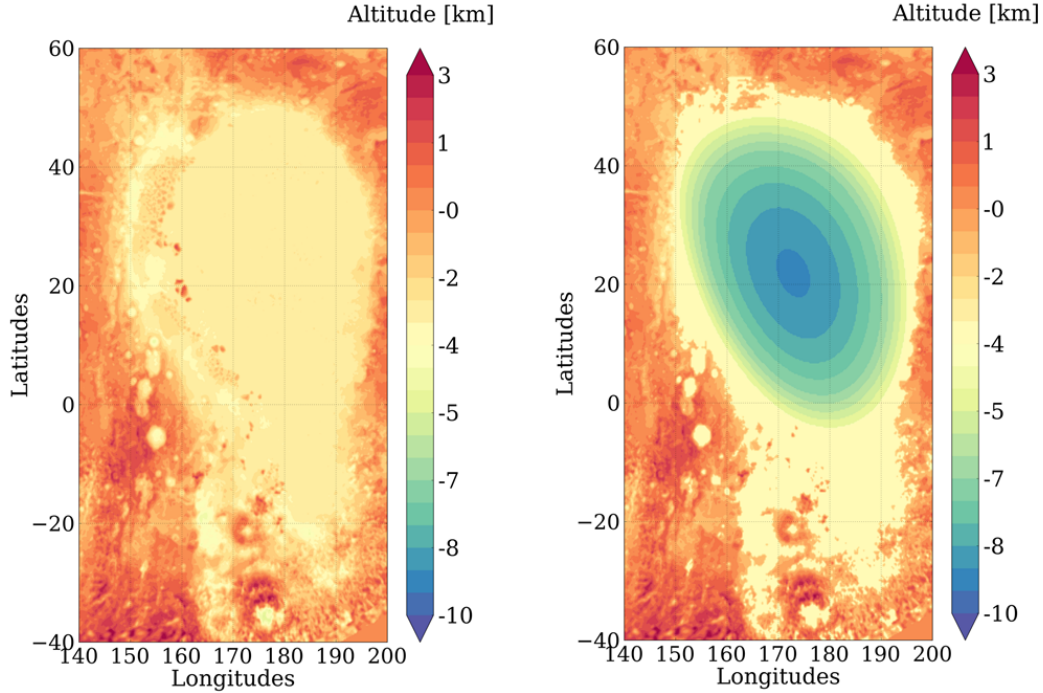


Fig. 2. Left: Topography of Sputnik Planitia as seen by New Horizons, filled by ice at 2.5 km below the mean surface (Schenk et al., 2016a,b). Right: The modeled initial topography of Sputnik Planitia with a 10 km deep bedrock (here not filled by nitrogen ice) assumed in the model.

387 reproduce with precision small glacial flows (e.g. in the narrow channels east
 388 of SP or around Tenzing Montes in the southern part of SP). Consequently,
 389 the model of glacial flow used in this paper does not intend to be quantita-
 390 tively accurate given its simplicity and the unknowns but instead intends to
 391 reproduce to first order the activity of the nitrogen glaciers (e.g. in Sputnik
 392 Planitia rapid flows in the centre of Sputnik Planitia and slow flows on the
 393 edges).

394 We use the scheme described in Umurhan et al. (2017) under the following
 395 assumptions. First, we consider that the ice within SP flows like pure nitrogen
 396 ice. Then, we consider the simple case of a laminar flow with an isothermal ice,
 397 without basal melting (thus we are in the case of a basally cold and dry glacier).
 398 This is typically valid for thin layers of ice (shallow ice-sheet approximation).
 399 In fact, a conductive temperature gradient of 15 K km^{-1} due to internal heat
 400 flux on Pluto is suggested in (McKinnon et al., 2016), assuming no convection.
 401 In that case, basal melting would occur below about 2 km of N_2 ice, assuming a
 402 surface temperature of 37 K. This 15 K km^{-1} value is probably an upper limit
 403 because of the convection within the ice. (McKinnon et al., 2016) suggest that

404 the ice layer is convecting in the so-called sluggish lid regime, which involves
 405 the entire layer of ice in the overturn. Therefore the ice temperature within
 406 the layer is likely colder than the temperature assumed without convection.
 407 (McKinnon et al., 2016) use a Nusselt number of 3.2, which means that the
 408 effective temperature gradient (in the horizontal mean) is rather 5 K km^{-1} .
 409 In that case, basal melting would occur below about 5 km of N_2 ice.

410 If the surface temperature of the ice has approached the melting temperature
 411 of 63 K at the triple-point of N_2 in the past, as suggested in (Stern et al.,
 412 2017), then it is likely that the thin layers of ice at the edges of the ice sheet
 413 were “temperate” glaciers at this time. However, our results show that during
 414 an entire astronomical cycle (even during high obliquity periods), the surface
 415 temperatures of nitrogen ice remain low, below 40 K (see Section 5.3), which
 416 reinforces our assumption of dry glacier at the edges of SP. Here we apply the
 417 case of a basally cold and dry glacier to all encountered ice thicknesses (with
 418 no internal heat flux and no basal melting). This is acceptable to first order
 419 because (1) our study focus on the edges of SP and on the glaciers outside SP,
 420 whose thickness in the model remains thin ($<1 \text{ km}$), (2) the large amount of ice
 421 in the centre of SP already flows extremely rapidly; a basal melting here would
 422 allow for even more rapid flow which would not significantly impact our results,
 423 (3) although the impact of internal heat flux on soil and surface temperature
 424 is not negligible ($+0.2 \text{ K}$ at the surface), it has a small effect on the flow
 425 compared to other parameters of the model, which are not well constrained,
 426 such as the albedo and the thickness of the ice (the glacial flow modelling
 427 strongly depends on the depth of the bedrock). We tested the model assuming
 428 that the effective temperature controlling the glacial flow is the one that we
 429 would obtain at the bottom of the glacier taking into account a conductive
 430 temperature gradient of 15 K km^{-1} (that is $\sim 55 \text{ K}$ for 1 km thick glacier),
 431 and it does not change significantly the results of this paper.

432 Finally, we consider that the bedrock remains static and is not altered by the
 433 glacial flow. Consequently, in the model, the ice is transferred from one grid
 434 point to another one using the modified Arrhenius-Glen analytic function of
 435 the mass-flux given in Umurhan et al. (2017):

$$436 \quad q_0 = g_Q \exp\left[\frac{\frac{H}{H_a}}{1 + \frac{H}{H_{\Delta T}}}\right] q_{glen} \quad (5)$$

$$437 \quad q_{glen} = A(\rho g)^n \frac{H^{n+2}}{n+2} \frac{\tan^{n-1}(\theta)}{(1 + \tan^2(\theta))^{\frac{n}{2}}} \quad (6)$$

438 With q_0 in $\text{m}^2 \text{ s}^{-1}$, g the gravity at Pluto’s surface (0.6192 m s^{-1}), H the
 439 ice thickness of the considered column of ice. ρ is the nitrogen ice density, set
 440 to 1000 kg m^{-3} (Scott, 1976; McKinnon et al., 2016; Umurhan et al., 2017).
 441 g_Q is a corrective factor given in Umurhan et al. (2017) and set to 0.5. H_a

442 and $H_{\Delta T}$ are parameters depending on the surface pressure and are given by
 443 equation 14 in [Umurhan et al. \(2017\)](#). θ is the angle between the two adjacent
 444 columns of ice (see Figure 7 in [Umurhan et al. \(2017\)](#)), and is defined by
 445 $\theta = \arctan(\Delta H / L_{ref})$, with ΔH the difference of altitude between both columns
 446 (computed from the bedrock topography and the amount of ice) and L_{ref} is the
 447 characteristic distance of the glacial flow (distance between both columns, that
 448 is both adjacent grid-points). The parameters A and n are given in [Umurhan](#)
 449 [et al. \(2017\)](#) are only depend on the surface temperature. By using this scheme
 450 in our model, we obtain the same relaxation times for the ice than those shown
 451 on Figure 8-9 in [Umurhan et al. \(2017\)](#) (the corresponding relaxation time of
 452 a 50 km long channel, sloping at $\theta = 10^\circ$ and initiated with 200 m of glacial
 453 ice is about 50 years). We adapted this scheme so that it fits on the model
 454 grid and so that each grid point can redistribute the correct amount of ice to
 455 the neighboring points.

456 **3 Orbital, obliquity and TI changes as drivers of surface tempera-** 457 **tures**

458 Obliquity is the main driver of insolation changes on Pluto. The polar regions
 459 receive more flux than the equator on annual average during high obliquity pe-
 460 riods and about the same flux than the equator during low obliquity periods.
 461 However, although one could think the rule also applies for surface tempera-
 462 tures, it is not systematically the case. The following paragraph explains why.

463 If one assumes that the surface temperature is only driven by the absorbed
 464 flux and the infrared cooling (neglecting the soil TI, the latent and sensible
 465 heat flux), then the surface temperature at equilibrium is given by:

$$466 \quad T_{eq} = \sqrt[4]{\frac{(1 - A)F}{\epsilon \sigma}} \quad (7)$$

467 with A and ϵ the surface albedo and emissivity respectively, F the absorbed
 468 flux and σ the Boltzmann constant. This equation shows that when the flux F
 469 strongly increases, the surface temperature only increases by a factor of $F^{1/4}$.
 470 In other words, the thermal infrared cooling limits the increase of surface
 471 temperatures.

472 As a result, the surface temperatures at the poles do not increase as much as
 473 the insolation during summer, and the poles can be colder than the equator on
 474 annual average, even if the mean insolation is not. This is true for low thermal
 475 inertia (< 800 SI), but not for medium-to-high TI, which enables the poles
 476 to store the heat accumulated during summer and release it during winter,

477 as illustrated on Figure 3. In the cases of TI between 800-1200 SI, the poles
 478 and the equator have similar surface temperatures and the coldest regions are
 479 around $\pm 30^\circ$ latitude. The higher the TI, the more equatorial are the coldest
 480 regions.

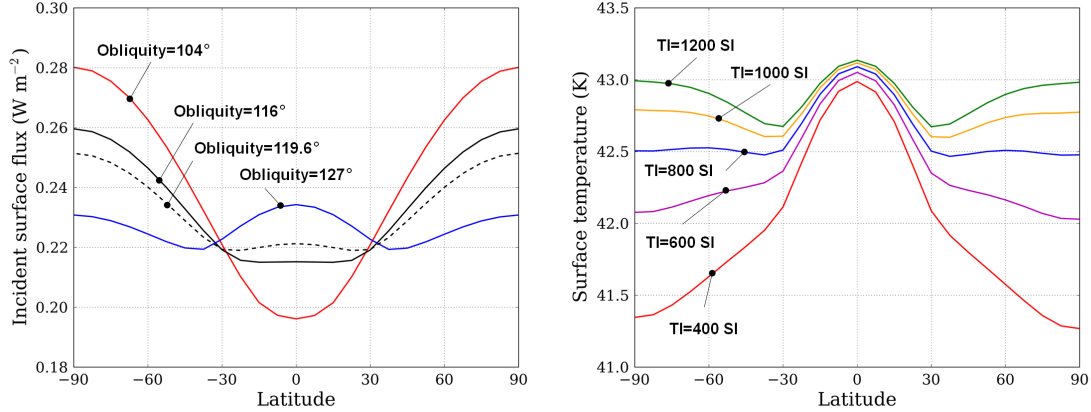


Fig. 3. Surface thermal model results. Left: Annual mean incident solar flux for an obliquity of 104° , 116° , 119.6° and 127° . Generally speaking, the poles receive more flux in average than the equatorial regions, except during the low obliquity periods (127°) where mid-latitudes receive less flux in average. Right: Annual mean surface temperatures obtained with the obliquity of 119.5° and the incident solar flux shown on the left panel, a $L_s \text{ peri}$ of 0° and TI of 400 SI (red), 600 SI (purple), 800 SI (blue), 1000 SI (orange), 1200 SI (green). The surface albedo is uniformly set to 0.1, and the emissivity to 1. The coldest points are the poles for the low TI case and the “low latitudes bands” at $\pm 30^\circ$ for the high TI case.

481 The variation of $L_s \text{ peri}$ is also significant because of the high eccentricity of
 482 Pluto’s orbit. In the past Myrs, the $L_s \text{ peri}$ parameter has created a North-
 483 South asymmetry of annual mean insolation and surface temperatures, favouring
 484 a warmer southern hemisphere when $L_s \text{ peri}$ values were close to 90° and
 485 a warmer northern hemisphere when $L_s \text{ peri}$ values were close to 270° (Fig-
 486 ure 4.A). The surface temperatures tend to be the same in both hemispheres
 487 for $L_s \text{ peri}$ values close to 0° and 180° .

488 The surface temperatures averaged over the last 14 Myrs (which corresponds
 489 to the last 5 obliquity cycles) and over the last 2.8 Myrs are shown on Fig-
 490 ure 4.B. For the same reasons mentioned above, the equatorial regions are
 491 colder than the poles for medium-to-high TI and warmer for low TI (< 800
 492 SI). For medium-to-high TI, the lowest temperatures are obtained at 30°N -
 493 45°N , which corresponds to the latitudes where a band of nitrogen ice has been
 494 observed by New Horizons. It can also be noted that the northern hemisphere
 495 is in average over several Myrs slightly colder than the southern hemisphere
 496 in all TI cases. This is because the last high obliquity periods of Pluto’s past

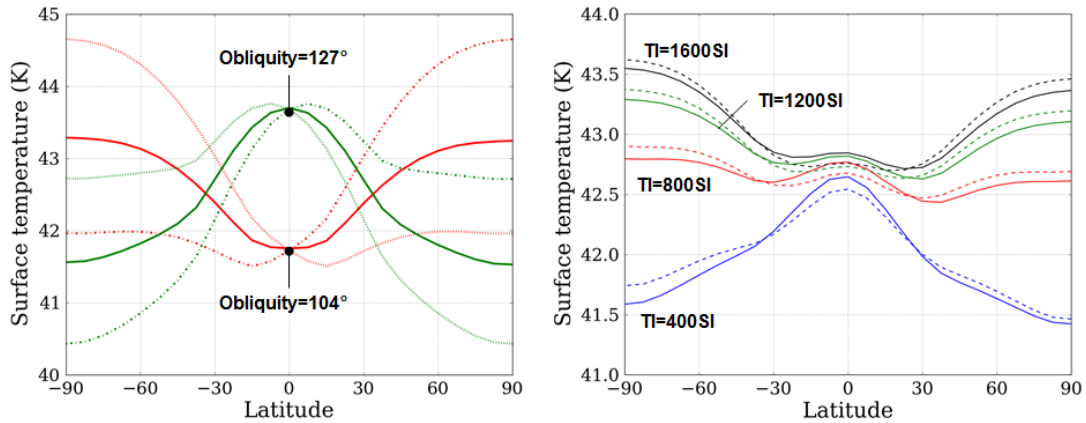


Fig. 4. Surface thermal model results. Left: Annual mean surface temperatures obtained assuming uniform and constant surface conditions (surface albedo = 0.1, TI=800 SI) for the maximum and minimum values of obliquities (red: 104°, green:127°) and $L_s \text{ peri}$ (solid line: 0°, dashed: 90°, dot-dashed: 270°). While the obliquity and the TI drive the location of the coldest region (polar or equatorial regions), the $L_s \text{ peri}$ induces an asymmetry of temperatures with $L_s=90^\circ$ and $L_s=270^\circ$ leading to a colder and warmer north pole respectively. Right: Surface temperatures averaged over the last 14 Myrs (last 5 obliquity cycles, solid lines) and 2.8 Myrs (last obliquity cycle, dashed lines) for different cases of TI. The surface albedo is uniformly set to 0.1, and the emissivity to 1. The polar regions are warmer than the equatorial regions, except in the case of TI lower than 800 SI. Our reference simulation (TI=800 SI) shows that the regions around $\pm 30^\circ$ are colder in average.

497 (during which the poles receive the most of insolation) remained coupled with
 498 a solar longitude at perihelion close to 90° , thus favouring colder northern
 499 latitudes during these periods and in average over several Myrs.

500 Assuming that the evolution of obliquity and $L_s \text{ peri}$ remained stable during the
 501 last billion of years, one can quantify the shift between the obliquity and the
 502 $L_s \text{ peri}$ values. As shown by Figure 5, between 260 and 165 Myrs ago, the $L_s \text{ peri}$
 503 during high obliquity periods varied from 225° to 315° , which favoured colder
 504 southern latitudes in average over several Myrs. Between 165 and 70 Myrs
 505 ago, the $L_s \text{ peri}$ during high obliquity periods varied from -45° to $+45^\circ$, leading
 506 to symmetric surface temperatures between both hemisphere in average over
 507 several Myrs. Finally, from 70 Myrs up to now, the $L_s \text{ peri}$ during high obliquity
 508 periods varied from 45° to 113° , which favoured colder northern latitudes in
 509 average over several Myrs. The entire period of the cycle obliquity+ $L_s \text{ peri}$ is
 510 375 Myrs.

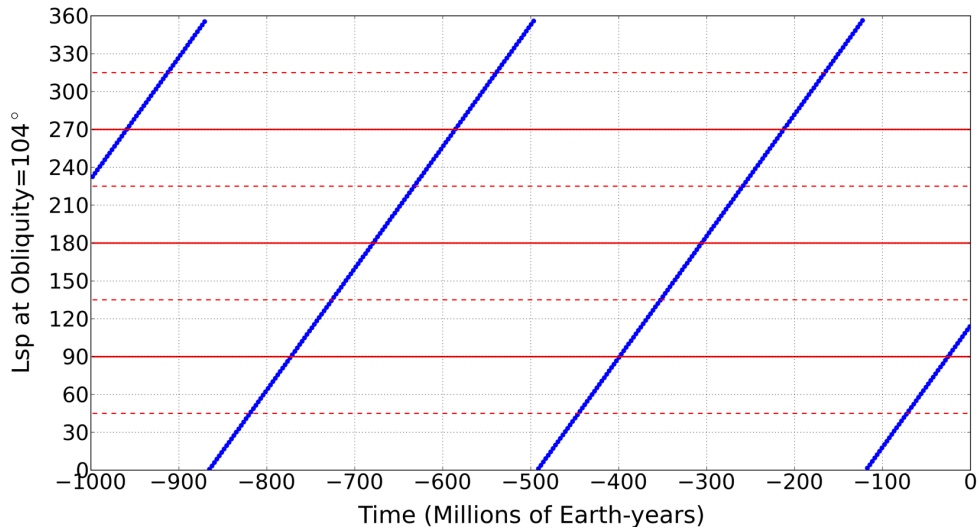


Fig. 5. Evolution of the solar longitude of perihelion ($L_{s \text{ peri}}$) at high obliquity (104°) during the last 1000 Myrs (assuming astronomical cycles stable with time). The $L_{s \text{ peri}}$ at high obliquity has been slowly shifted with time, e.g. from 110.8 to 113.4° during the last 6 Myrs, due to the slight difference of periods between both $L_{s \text{ peri}}$ and obliquity cycles. During the last 70 Myrs, the $L_{s \text{ peri}}$ value at high obliquity remained close to 90° and thus lead to an asymmetry of insolation and surface temperatures favouring a slightly warmer south hemisphere (see Figure 4).

511 4 Exploring the changes of N_2 ice thickness in Sputnik Planitia

512 In this section, we explore the past evolution of the N_2 ice thickness within
 513 Sputnik Planitia using the volatile transport model in the configuration as
 514 described above and with all of the initial N_2 ice reservoir sequestered in
 515 the deep Sputnik Planitia basin. We explore the changes of N_2 ice thickness
 516 considering its condensation and sublimation cycles, first without glacial flow
 517 (Section 4.1) and then with glacial flow (Section 4.2). In this paper we assume
 518 a compact N_2 -rich ice so that 1 kg of ice per m^2 corresponds to a thickness of
 519 1 mm .

520 4.1 The cycles of condensation and sublimation

521 We first start the simulation 30 Myrs ago with nitrogen ice sequestered in
 522 SP and let the amount of ice evolve at the surface. In this section, we do
 523 not perform the simulations with glacial flow. Instead, we assume that the
 524 timescale for ice viscous flow is very short and that the ice sheet surface is
 525 effectively a level sheet, remaining flat at all times, and we only evaluate the
 526 condensation and sublimation rates within SP. Note that in this simulation,

527 no nitrogen frost form outside SP.

528 Figure 6 shows the net change of N₂ ice thickness obtained with the model
529 over four different timescales: A, one Pluto day in July 2015; B, one current
530 Pluto year; C, during the last 500 000 Earth years, which correspond to the
531 estimated time of full resurfacing of SP by the action of the convection cells
532 ([McKinnon et al., 2016](#)); D, during the last 2.8 Myrs (last obliquity cycle).
533 These results are compared with geologic features observed by New Horizons
534 within SP (Figure 6.E-F).

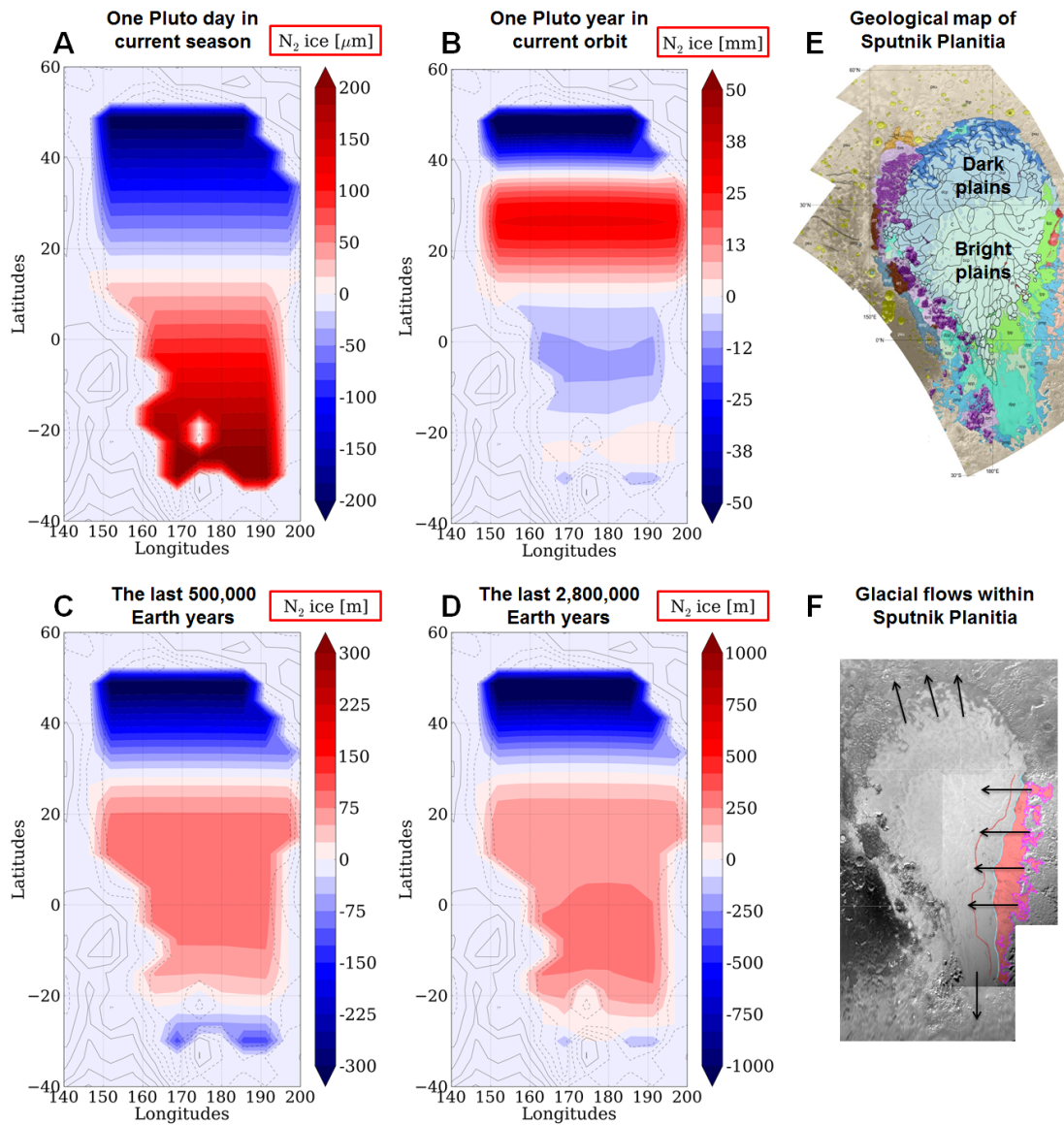


Fig. 6. Sublimation-condensation rates of N_2 (zoom at Sputnik Planitia) at different timescales (note the order of magnitude differences between the colorbars, from μm to m): (A) During one Pluto day in July 2015. (B) During one Pluto year in current orbital conditions. (C) During the last 0.5 Myrs. (D) During the last 2.8 Myrs (obliquity cycle). (E) Geological map of the Sputnik Planitia region (a full resolution version can be found in [White et al. \(2017\)](#)). (F) New Horizons mosaic of Sputnik Planitia, with recent glacial activity indicated by the red area. The purple line indicates the extent of the N_2 ice sourced for the glaciation, the cyan line indicates the current ice deposition limit, and the red line indicates the inferred former ice deposition limit. The black arrows indicate the direction of the flow. Originally shown as Fig. 6 in [Howard et al. \(2017\)](#).

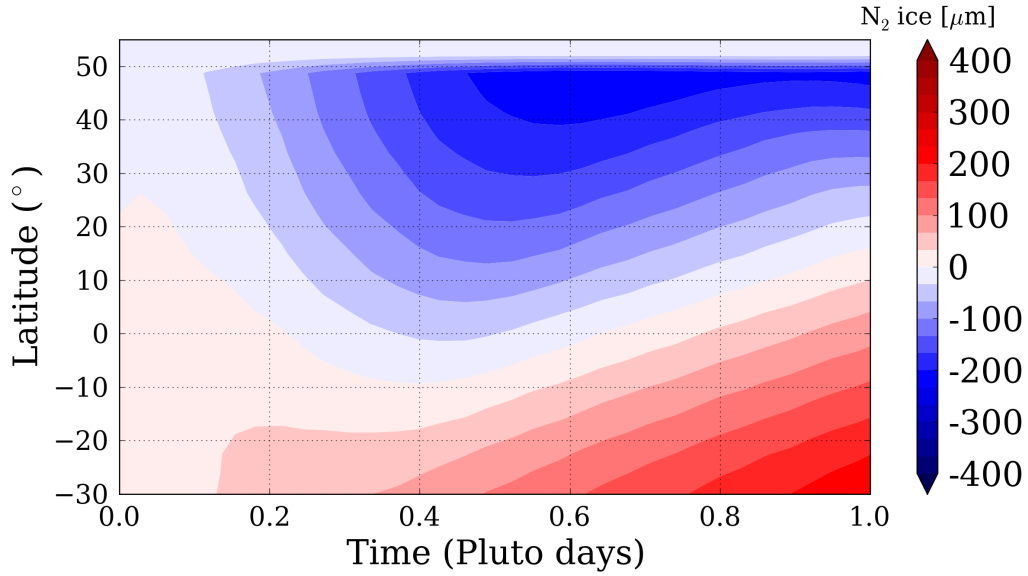


Fig. 7. Variations of N_2 ice thickness within Sputnik Planitia, during one Pluto day in July 2015, normalized to 0 at $t=0$. The data is taken at the longitude 180° , where the ice covers the latitudes 30°S - 50°N . As shown by Figure 6, the flux does not vary with longitude within Sputnik Planitia.

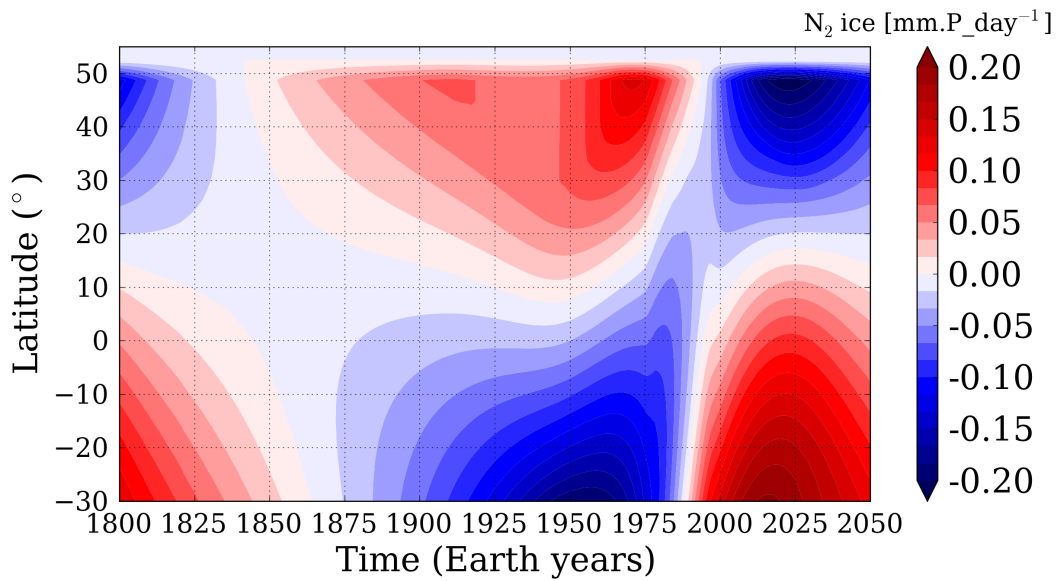


Fig. 8. Evolution of the diurnal mean condensation-sublimation rate within Sputnik Planitia (mm per Pluto day), in current orbital conditions, from 1800 to 2050 assuming that the glacier remains flat.

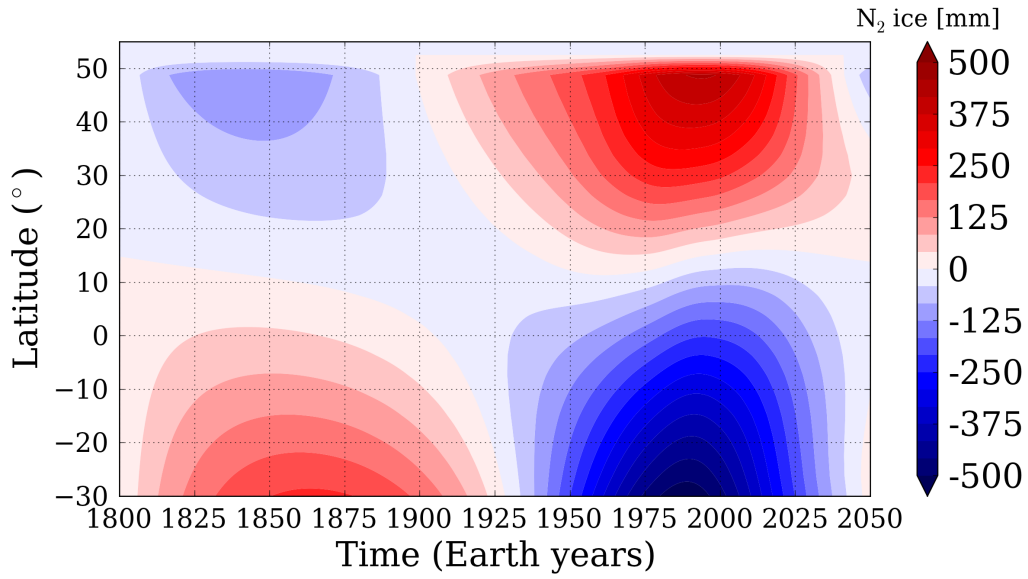


Fig. 9. Variations of N_2 ice thickness within Sputnik Planitia (normalized to 0 at $t=1800$), in current orbital conditions, from 1800 to 2050 assuming that the glacier remains flat. The data is taken at the longitude 180° . Although the net budget of ice within one Pluto year varies by tens of mm (Figure 6.B), the thickness of ice involved during this year reaches hundreds of mm.

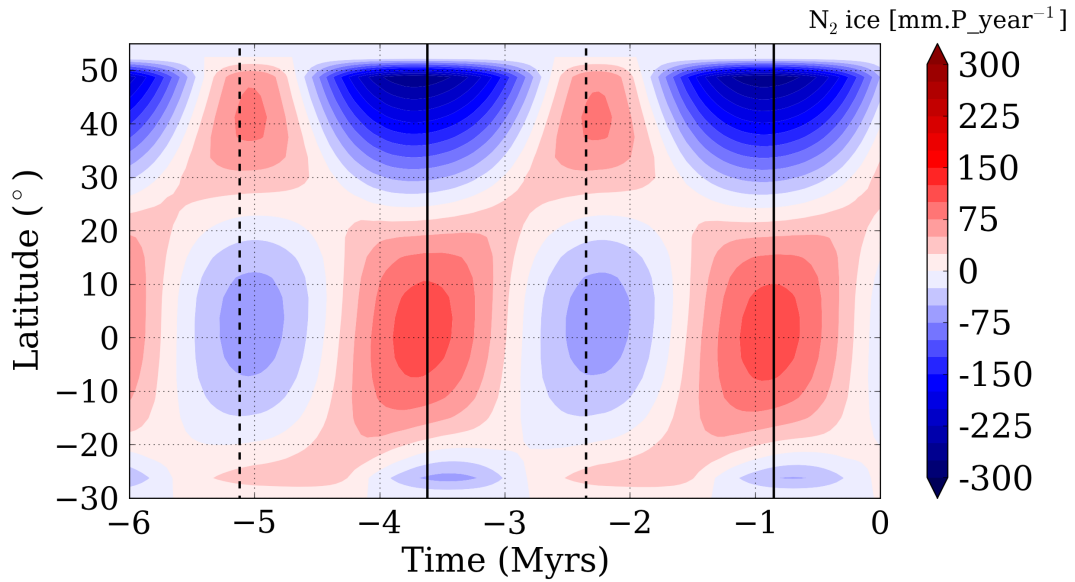


Fig. 10. Evolution of the annual mean condensation-sublimation rate of N_2 ice with time (mm per Pluto year), assuming that the glacier remains flat (same as Figure 8). The vertical solid and dashed lines correspond to the periods of high (104°) and low (127°) obliquity respectively.

535 *4.1.1 The current annual timescale*

536 Figure 7 shows the normalized diurnal variations of N₂ ice thickness over
537 a Pluto day in July 2015. Figure 8 shows the evolution of the diurnal mean
538 condensation-sublimation rate (net change of N₂ ice thickness) within Sputnik
539 Planitia, over one current Pluto year, since 1800, while Figure 9 shows the
540 normalized variations of N₂ ice thickness at same dates (gross change of N₂
541 ice thickness).

542 Over one Pluto day, several tens of micrometres of nitrogen ice move from
543 the summer (North) to the winter (South) parts of SP (Figure 6.A, Figure 7),
544 while in one current Pluto year, a net amount of 20-50 mm of ice accumulates
545 around 30°N, 10-15 mm are lost in the southern part (< 10°N) and 20-50 mm
546 are lost in the northern edge of SP (> 40°N, Figure 6.B).

547 In 2015, the regions above 15°N are in a sublimation-dominated regime, while
548 regions below 15°N are in a condensation-dominated regime (Figure 6.A, Fig-
549 ure 8). The southern regions of SP entered the condensation-dominated regime
550 after the northern spring equinox in 1988, where a fast transition of regime
551 between the northern and southern regions occurred. Before 1988, the south-
552 ern regions had been in a sublimation-dominated regime since 1865. The net
553 variation of ice thickness after one Pluto year reaches tens of mm (Figure 6.B,
554 Figure 8) but the sublimation-condensation during this period involves thicker
555 layers of ice (by a factor 10-30, Figure 9). Between 1865 and 1988 (7033 Pluto
556 days), the southern regions lost 0.3-1 m of N₂ ice. Between 1988 and 2015, the
557 regions below 10°S accumulated 0.15-0.25 m of N₂ ice.

558 **Association with the observed pits south of Sputnik Planitia** Figure 10
559 shows the annual mean condensation-sublimation rates over the last 6 Myrs.
560 The southern latitudes of SP (20°S-10°N) are in a sublimation-dominated
561 regime since at least 100 000 years. The region below 20°S is a sublimation-
562 dominated regime since 1.3 Myrs and currently starts to enter a condensation-
563 dominated regime. The net loss of ice involved at the annual timescale in
564 these regions occurs in the model at the same latitudes where the small pits
565 are observed, explaining their formation there if they formed by sublimation.
566 Between 20°S-10°N, if we assume relatively similar insolation conditions over
567 the last 100 000 Earth years, with a mean net sublimation rate of 15 mm of N₂
568 ice per Pluto year (Figure 6.B), then the total loss of ice in this region could
569 reach 6 m. Below 20°S, assuming a mean sublimation rate of 50 mm of N₂
570 ice per Pluto year (Figure 10) over 1.3 Myrs, the loss of ice reaches ~ 260 m.
571 These values are in accordance with the observed depth of the pits (tens of
572 meters, [Moore et al. \(2017\)](#)). Other mechanisms not taken into account in
573 this model, such as atmospheric winds, light reflection and deposition of dark
574 materials at the bottom of the pits may further increase the sublimation rate
575 and favor deeper pits formation. This annual mean sublimation pattern could

576 also explain the disappearance of the polygonal cells (if they are erased by
577 sublimation), although this may also be related to a lower ice thickness (too
578 low to trigger convection), as it is probably the case for all edges of SP.

579 **Association with the ice albedo and composition** Our results also show
580 that the latitudes where N_2 ice accumulates in average over one Pluto year
581 (Figure 6.B) correspond to the latitudes where bright N_2 plains and a weaker
582 amount of CH_4 in the N_2 - CH_4 mixture (both are correlated) are observed in SP
583 (Protopapa et al., 2017; Schmitt et al., 2017; Buratti et al., 2017). Protopapa
584 et al. (2017) note that the abundance of $N_2:CH_4$ is higher at the center of
585 Sputnik Planitia with respect to the northern area of the basin, contrary to
586 the dilution content of CH_4 in the mixture (Figure 11). They interpret this
587 trend in the composition maps as a possible north-south sublimation transport
588 of nitrogen in Sputnik Planitia (indicated schematically by the arrow in panel
589 B of Figure 11). This is now supported by our results showing a net deposition
590 of N_2 ice in the middle of the basin over the seasonal timescales (Figure 6.B),
591 and a recent deposition of few micrometers of N_2 ice in the southern latitudes
592 during the past 30 Earth years (Figure 8).

593 Despite its net daily sublimation since about 30 Earth years (Figure 8), the
594 darker cellular plains are currently an area of net ice accumulation on the
595 annual timescale (about 4-8 m in the last 100 000 Earth years, Figure 6.B and
596 Figure 10), explaining why they also remain relatively bright compared to the
597 northern dark trough-bounding plains (above $40^\circ N$), which are subjected to
598 net annual sublimation since almost 1.8 Myrs (Figure 10).

599 4.1.2 *The astronomical timescale*

600 Figure 6.D shows that over the last obliquity cycle (2.8 Myrs ago up to now),
601 up to 300 m of N_2 ice accumulated between $20^\circ S$ - $30^\circ N$, while an intense loss of
602 about 1 km of ice occurred at the northern edge of the ice sheet between $30^\circ N$ -
603 $50^\circ N$. In addition, at the southern edge of SP (below $20^\circ S$), a net loss of 150
604 m of ice also occurred. As shown by Figure 10, N_2 sublimation at the northern
605 edge of SP is the most intense during the periods of high obliquity (e.g 0.85
606 Myrs ago), and still occurs there during a large part of the obliquity cycle, for
607 obliquities lower than 119° (higher than 61° in retrograde rotation). As shown
608 by Figure 6.C, during the last 0.5 Myrs, the mean accumulation and loss of
609 ice occurred at similar latitudes than during the last 2.8 Myrs, except between
610 $15^\circ S$ - $20^\circ S$ since these latitudes are currently transitioning to a sublimation-
611 dominated regime. During the last 0.5 Myrs, the center of SP accumulated
612 up to 100 m of ice while the northern regions lost 200-300 m of ice, that is

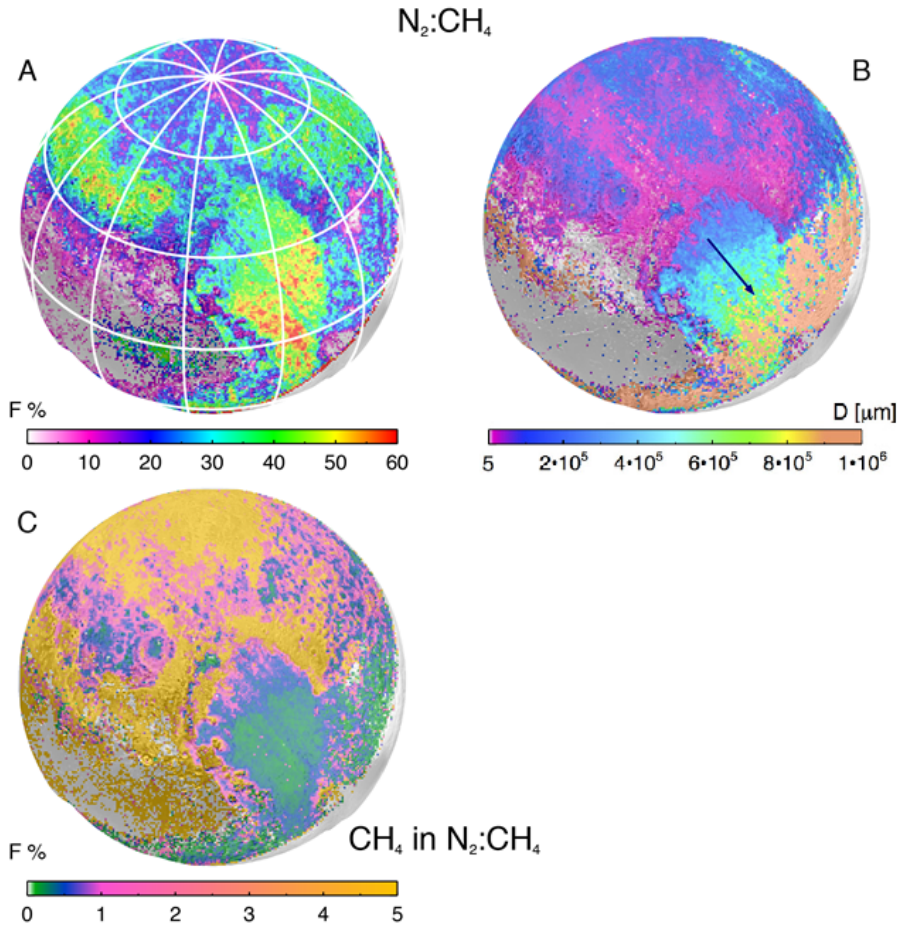


Fig. 11. Modeling results from [Protopapa et al. \(2017\)](#) showing the abundance (A) and the path length (B) of the N₂-enriched. Panel C shows the dilution content of CH₄ in N₂.

613 one third of what they have lost in average over the last obliquity cycle (2.8
 614 Myrs). Note that a net loss of ice continuously occurs at the northern edge of
 615 SP since the last 1.8 Myrs. During the same period, ice has been continuously
 616 condensing between 20°S-25°N. We can associate several structures of SP to
 617 the change of N₂ ice thickness averaged over this astronomical timescale.

618 **Depressions and outward glacial flows at the northern and southern**
 619 **edge of Sputnik Planitia** First, the latitudes where 1-2 km deep depressions
 620 are observed at the northern and southern boundaries of the ice sheet (see
 621 Figure 8 and 17 in [Howard et al. \(2017\)](#)) coincide with the latitudes where
 622 intense sublimation of ice occurred in the last 2.8 Myrs. This loss of ice should
 623 tend to be compensated by glacial flow, in line with the outward direction of
 624 the flow observed at these edges, and with the evidences of the particularly
 625 strong erosion of the Al-Idrisi Montes at the northern edge of SP ([Howard](#)
 626 [et al., 2017](#)). Simulations with glacial flow are explored in Section 4.2.

627 **Recent glacial activity at the eastern side of Sputnik Planitia** Sec-

628 ondy, the recent glacial activity of ice flowing westward through the valleys
629 of the eastern side of SP (pink color on Figure 6.F, the observations show
630 that the ice at the eastern side of SP flows toward the center of SP) occurs
631 at the same latitudes where nitrogen ice continuously accumulated during the
632 last 1.8 Myrs (20°S-30°N). We suggest that the accumulation of ice at these
633 latitudes created a topography gradient at the edge of SP as the thick layer of
634 ice far from the edge (closer to the center of SP) flowed more rapidly than the
635 shallow one at the edge. These glacial flows should be reduced or disappear
636 during the next hundreds of thousand years since these latitudes gradually
637 enter a sublimation-dominated regime (Figure 10).

638 Why are such glacial flows not observed on the western side of SP, where the
639 latitudes receive the same insolation? Glacial activity on the western side of
640 SP has occurred as evidenced by the many erosional valleys, but these valleys
641 are not filled with flowing ice like they are to the east. This could be due
642 to the significant difference of geology between the western and eastern side.
643 As shown by [Schenk et al. \(2018a\)](#), a North-South giant fault system passes
644 under the western edge of the ice sheet, which may explain the fragmentation
645 of water ice blocks and the presence of deep ridge, faults, and cliffs observed
646 on the western edge of SP. This topography may prevent the ice from flowing
647 easily through the west side of SP and form large glacial flows. In addition, the
648 western side of SP may correspond to a deeper bedrock than on the eastern
649 side, preventing strong gradients of nitrogen ice thickness and the inward flow
650 observed in the eastern raising valleys (the ice would locally flow faster on the
651 western edge of SP).

652 **The dark northern plains of Sputnik Planitia** The dark and methane
653 rich aspect of the northern edge of Sputnik Planitia (40°N-50°N) is also con-
654 sistent with our results, which show that this area is a sublimation area at all
655 timescales: the current diurnal, the current annual, the last 0.5 Myrs and the
656 last 2.8 Myrs. Why does this area not have small pits, like in the southern
657 part of SP? A suggestion is that the area lacks an intake of fresh nitrogen ice
658 necessary for the formation of pits. This may be because the area is subject
659 to a net loss of ice at all timescales and the layer of ice became too shallow to
660 undergo solid-state convection. In addition or alternatively, the methane rich
661 composition and the size of grains of this dark ice may play a restricting role
662 in the formation of pitted plains. Finally, the formation of pits is a process of
663 erosion by reflected light. If the ice albedo is too low, the direct absorption
664 of solar energy predominates the reflection and the ice sublimates uniformly,
665 inhibiting the pit formation ([Moore et al., 2017](#)).

666 *4.2 The astronomical cycles with glacial flow*

667 In this section, we repeat the same simulations as in Section 4.1 except that
668 we turn on the glacial flow scheme of N₂ ice (described in Section 2.5), which
669 enables the ice to flow in the modelled Sputnik Planitia basin (Section 2.4).
670 The basin is initially filled with N₂ ice up to 2.5 km below the mean surface
671 level. We assume that the edges of the basin are at about 3 km, 4 km or 5 km
672 below the mean surface level (Figure 2).

673 *4.2.1 General overview*

674 As a general tendency, our results show that over one obliquity cycle, only
675 small variations of elevation up to 25 m are obtained in the centre of SP at 20°N
676 (SP remains relatively flat where the ice is thick) while variations of elevations
677 of 200-300 m are obtained at the edges of SP (Figure 12 and Figure 13), in
678 particular at the northern and southern edges. The variations are reduced
679 if we assume the bedrock deeper below the ice sheet. These variations of
680 elevation obtained with our model are consistent with the depressions observed
681 at the northern and southern boundaries of SP and with the eroded mountain
682 blocks observed west and east of Tenzing Montes, indicative of the presence
683 of large amounts of ice there in the past. Figure 12 suggests that the ice
684 sheet was at its maximal North-South extension 1.5-2 Myrs ago, since the
685 ice level in the Al-Idrisi region and in the far south of SP was well above
686 the level of the centre of SP. Conversely, the last million of years coincides
687 with a period of minimal extension, which is consistent with the ice flowing
688 outward from SP at its northern and southern edges (Howard et al., 2017)
689 and the lower MVIC-derived topography observed north of the Al-Idrisi region
690 (Schenk et al., 2018b).

691 *4.2.2 Comparisons with observations*

692 **The Al-Idrisi Montes** As shown by Figure 13, the entire northern part of
693 SP (above 40°N) is subject to variations of altitudes of 100-280 m, which is
694 consistent with the intense sublimation and condensation of N₂ ice occurring
695 over one obliquity cycle at these latitudes (Figure 6.C-D). In particular, the
696 latitudes of the Al-Idrisi Montes displays one of the largest variations of ele-
697 vations (up to 280 m), in agreement with the scenario of strong and endless
698 erosion of the water ice blocks in this region (Figure 12 and Figure 13). In
699 the simulation with the less deep bedrock on the edges of SP, the ice at the
700 latitudes of the Al-Idrisi Montes sublimed during the last 2 Myrs and revealed
701 the bedrock (which is 2.55 km below the mean surface at this location in that
702 case, Figure 12 red dotted line). Currently, this region enters a regime of net

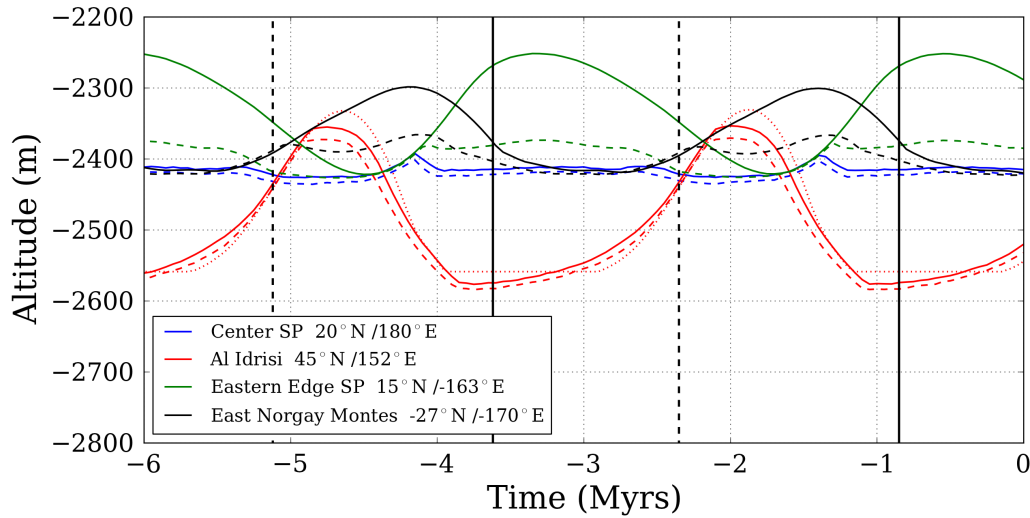


Fig. 12. Variations in elevation within SP at different locations, assuming that the bedrock below SP include a 6-9 km deep elliptical basin and edges at 4 km (solid lines) and 5 km (dashed lines) below the mean surface level. The red dotted line corresponds to a case with edges at about 3 km below mean level. In that case, the ice has been entirely sublimed during the last millions of years at Al-Idrisi, as the elevation shown during that time is the bedrock level at this location (flat line at 2.55 km below the mean surface). The vertical solid and dashed lines correspond to the periods of high (104°) and low (127°) obliquity respectively.

704 **The recent glacial activity at the eastern side of Sputnik Planitia**

705 Figure 12 also shows the evolution of the ice at the eastern edge of SP, at 15°N .
 706 As predicted by Figure 10, the area accumulated up to 150 m of ice during
 707 the high obliquity periods, if the bedrock is at 4 km below mean surface (the
 708 variation is less if the bedrock is deeper). The elevation of this area decreases
 709 since 0.6 Myrs because the flow of ice toward the center of SP overcomes the
 710 intake of nitrogen from condensation. Note that this area is always higher
 711 than the center of SP. Thus, the glacial flows induced from the uplands to the
 712 center of SP, as observed by New Horizons, should never stop.

713 **The southern latitudes of Sputnik Planitia**

714 The south of SP also displays strong variations of elevation, that are about 200 m over one obliquity cycle,
 715 with a bedrock at 4 km below mean surface (Figure 13). At the east of the
 716 Tenzing Montes ($27^\circ\text{S}, -170^\circ\text{E}$), the elevation of the ice is higher than the center
 717 of SP during most of the obliquity cycle.

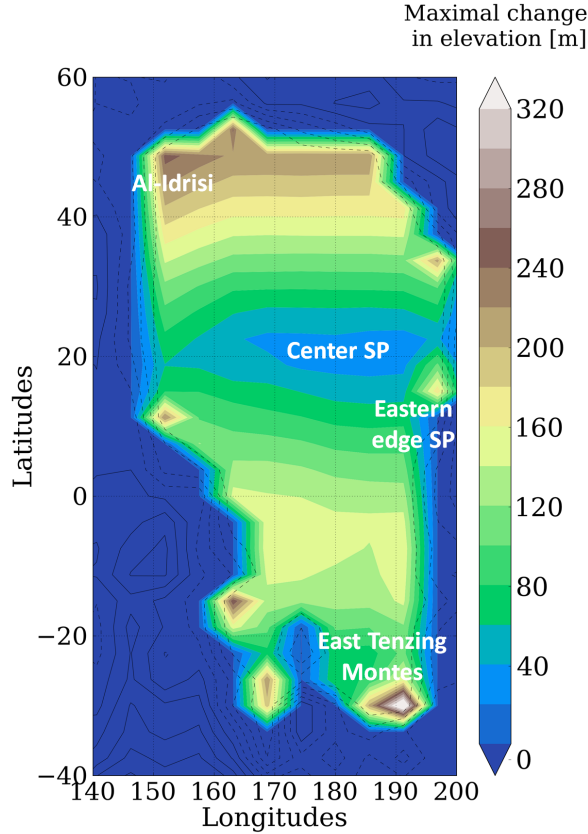


Fig. 13. Maximal variation in elevation of N_2 ice over the last obliquity cycle (last 2.8 Myrs), with a bedrock on the edges of SP at 4 km and an initial filling of SP at 2.5 km.

718 5 Possible steady-state conditions for Pluto's ices

719 In this section, we explored the stability of N_2 ice deposits outside Sputnik
 720 Planitia. To do that, we performed several simulations using different sensi-
 721 tivity parameters and initial states.

722 5.1 Simulation settings

723 We used the following settings for the simulations: (1) We performed the
 724 simulations over the last 30 Myrs, taking into account the obliquity and orbital
 725 changes over time described in Section 1. (2) We used realistic reservoirs of
 726 N_2 ice corresponding to a global surface coverage of Pluto of 200 m, 500 m or
 727 1000 m of ice. The case of 500 m corresponds to a basin of 1200x1000 km filled
 728 by ~ 7 km of ice, which is in the range of what is assumed for SP. (3) At the

729 beginning of these simulations 30 Myrs ago, the surface is not initialized with
730 the entire N₂ reservoir trapped inside SP as in Section 4. Instead, the initial N₂
731 reservoir is either globally uniformly distributed (Simulations #Glob), or placed
732 at the equatorial regions between $\pm 30^\circ$ latitude (Simulations #Equa), or at
733 the poles above 50° latitude (Simulations #Polar). As an example, an initial
734 global reservoir of 500 m redistributed over the equatorial regions between
735 $\pm 30^\circ$ latitude corresponds to an initial equatorial reservoir of ~ 1 km of ice.
736 (4) We used the latest topography data from New Horizons coupled with a
737 deep bedrock for SP (up to 10 km deep), as described in Section 2.4, and the
738 glacial flow scheme described in Section 2.5.

739 The sensitivity parameters of the simulations are the following: (1) Seasonal
740 thermal inertia of 400, 800 and 1200 SI are used, similar than those used in
741 [Bertrand and Forget \(2016\)](#). The diurnal thermal inertia remains fixed at 20 SI
742 ([Lellouch et al., 2011](#)), as in [Bertrand and Forget \(2016\)](#). (2) The reference N₂
743 albedo and emissivity used are set to 0.7 and 0.8 respectively, while those for
744 bare ground are set to 0.1 and 1 respectively, which is in the range of what
745 has been used in [Bertrand and Forget \(2016\)](#), assuming the water ice bedrock
746 is covered by dark tholins. We also explored the case of an albedo of 0.4 for
747 N₂ ice.

748 5.2 Simulation results

749 The results are summarized in Table 1 and illustrated by Figure 14 and Fig-
750 ure 15.

751 5.2.1 Overall outcome

752 As a general rule, N₂ ice quickly accumulates in the Sputnik Planitia basin
753 and in the equatorial regions (preferentially at latitudes around $\pm 30^\circ$), with
754 stronger condensation rates inside SP and inside other depressions because of
755 the stronger infrared cooling effect, as detailed in Section 1 and [Bertrand and](#)
756 [Forget \(2016\)](#).

757 However, in many of the simulations, large deposits also remain in the equato-
758 rial regions outside SP after 30 Myrs, and even beyond as they seem to remain
759 relatively stable with time. The simulation #Polar8 described in Table 1 and
760 shown on Figure 14 provides a typical example. Starting with an initial global
761 reservoir of 500 m confined at the poles and a thermal inertia of 1200 SI, the
762 ice migrates toward the equatorial regions by forming latitudinal bands which
763 get closer to the equator with time. The basin SP is progressively filled by N₂
764 ice, with a decreasing rate with time, because the ice outside SP migrates to-

765 wards the more stable equatorial regions, leading to lower condensation rates
 766 inside SP, and also because as the surface of the basin becomes less deep, the
 767 infrared cooling effect becomes less efficient. The parameter $\tau_{95\%}^{SP}$ indicates the
 768 time needed to fill SP at 95% of its final state (in Myrs). It depends on the
 769 TI, the reservoir and the initial state. The lower this time, the more stable are
 770 the deposits outside SP. As an example, in the simulation #Polar8, the basin
 771 is already in a relatively stable state after 11.90 Myrs. After 30 Myrs, it is
 772 filled by ice up to 2350 m below the mean surface (Table 1). Outside SP, N₂
 773 ice remained at the equator forming 600-800 m deposits. After these 30 Myrs,
 774 the ice still migrates in the basin because of the infrared cooling effect but at
 775 a very slow rate. Typically, in 1 Myrs, the equatorial deposits lost 5-10 meters
 776 of ice. Consequently, the 600-800 m deposits outside SP should end trapped
 777 inside SP after at least 60 additional Myrs.

778 We note that the ice in the equatorial regions outside SP is slightly less stable
 779 for L_s *peri* values close to 90° and 270° (values favouring an asymmetry of
 780 surface temperatures between both hemisphere). Finally, N₂ ice is never stable
 781 at the poles and any initial polar deposit up to 1 km thick is entirely sublimed
 782 after less than 2 Myrs.

783 5.2.2 Sensitivity to the ice reservoir

784 The larger the ice reservoir, the faster the glacial flow and the more easily the
 785 ice reaches the equatorial regions (outside SP), where it is able to form rela-
 786 tively stable deposits several hundred meters deep. In addition, larger reser-
 787 vairs of ice lead to larger N₂ ice deposits outside SP, spread from the equator
 788 toward higher latitudes.

789 In our simulations, equatorial deposits outside SP inevitably form as soon as
 790 the initial reservoir is equal to or larger than 500 m, independently of any
 791 initial distribution as long as it is assumed that the initial reservoir is outside
 792 SP. If the initial reservoir is lower, the ice does not flow easily and the presence
 793 of equatorial deposits outside SP depends on the TI and the initial state (see
 794 section 5.2.3).

795 As an example, in the simulations #Polar4 and #Polar7 performed with a reser-
 796 voir of 200 m of ice, all the ice ends in the SP basin after 30 Myrs (see Fig-
 797 ure 14) and fills it up to 3.29 km below the mean level. If the 200 m of ice are
 798 initially present at the equator (Simulation #Equa and #Glob), and if the TI is
 799 higher than 800 SI then 200-400 m thick ice deposits can persist in the equa-
 800 torial regions after 30 Myrs (e.g. simulations #Glob4, #Glob7, #Equa4, #Equa7,
 801 see Table 1).

802 While in the simulations performed using a reservoir of 200 m the SP basin is

803 filled by ice up to 3.29 km below the mean level after 30 Myrs, in all simulations
804 using a reservoir of 500 m of ice, the SP basin is filled up to 1500-2300 m below
805 the mean level. In all simulations using a reservoir of 1 km of ice, the basin is
806 entirely filled with ice. In these cases, the basin fills up very rapidly because
807 a large amount of ice is able to flow directly inside the basin.

808 5.2.3 Sensitivity to thermal inertia and initial state

809 Our results are sensitive to the assumed thermal inertia. As shown by Figure 3
810 and Figure 4, the lower the TI, the less equatorial are the cold points on Pluto's
811 surface (in average over the last Myrs). In particular, if TI is lower than 800
812 SI, the equator becomes warmer in average than the other latitudes. In the
813 simulations using a reservoir of 200 m of ice, different final states are obtained
814 after 30 Myrs depending on the TI and the initial state.

815 (1) If the initial reservoir is distributed at the poles (`#Polar1`, `#Polar4`, `#Polar7`),
816 we found that the ice subsists outside SP after 30 Myrs only if the TI is equal
817 to or lower than 400 SI, where a relatively stable latitudinal band of 330 m
818 N₂ ice can form at 20°N (`#Polar1`, Figure 14). If the TI is larger (`#Polar4`,
819 `#Polar7`), the entire reservoir is quickly trapped in SP (Figure 14).

820 (2) If some of the initial reservoir is distributed at the equator (`#Equa`, `#Glob`),
821 the ice can remain outside SP after 30 Myrs only if the TI is equal to or
822 larger than 800 SI. The ice forms latitudinal bands of 300-800 m N₂ ice at the
823 latitudes $\pm 10^\circ$, with higher amounts in the local depressions (see Figure 15,
824 `#Glob4` and `#Glob7`). If the TI is lower (`#Glob1`, `#Equa1`), the ice is less stable at
825 the equator and ends trapped in the SP basin (Figure 15). Generally speaking,
826 results obtained using an initial ice reservoir distributed at the equator and
827 over the globe are similar and therefore we only show the latter results on
828 Figure 15. Note that when larger TI are used, larger amounts of ice remain in
829 the equatorial regions. In addition, the deposits tend to peak at the equator
830 for large TI, while they tend to peak at higher latitudes ($\pm 10^\circ$, or $\pm 20^\circ$) for
831 low TI (see e.g. `#Polar1`, `#Glob4`).

832 5.2.4 Sensitivity to the albedo

833 The simulations using a reservoir of 500 m of ice have also been performed us-
834 ing an albedo of 0.4 for N₂ ice (`#Polar10-12`, `#Equa10-12`, `#Glob10-12`), instead
835 of 0.7 (reference value). In all these low albedo simulations, the ice sublimates
836 very rapidly from the poles and accumulates in the equatorial regions between
837 37.5°S and 37.5°N (the ice is slightly more spread than in the cases with an

838 albedo of 0.7), forming stable deposits about 600-800 m deep. These results
839 are found to be relatively independent of the initial state and of the thermal
840 inertia. This is because the lower albedo enables the ice to be warmer and to
841 gain greater mobility (by both glacial flow and condensation-sublimation flux)
842 to reach the coldest point on Pluto's surface.

843 In these simulations, SP is rapidly filled by ice and reaches a relatively stable
844 level. After $\tau_{95\%}^{SP}=7-9$ Myrs, the elevation of SP surface then increases by only
845 a few meter every Myrs due to N₂ ice condensation.

846 5.3 Minimum and maximum surface pressures

847 Figure 16 shows the evolution of the maximum and minimum annual surface
848 pressures during the last 15 Myrs obtained in simulations #Polar1, #Polar4,
849 #Polar8 and #Polar12. Generally speaking, the surface pressures (and surface
850 temperatures) remain within 10⁻²-10 Pa (31-40 K) in all simulations using
851 an albedo for N₂ ice of 0.7, and within the range 1-100 Pa (39-45 K) in all
852 simulations using an albedo for N₂ ice of 0.4 (in the model we are always
853 in the global-atmosphere regime). Higher maximum surface pressures could
854 be obtained, if we lower the albedo below 0.4 or the TI below 400 SI, but
855 such values seem quite distant from reality. We note that (1) there are two
856 peaks of maximum surface pressure per obliquity cycle (2) Maximum pressures
857 are lower during the high obliquity periods (104°). This is because the main
858 reservoirs of ice are located in the equatorial regions, which receive less flux
859 on annual average during these periods (Figure 3) (3) The surface pressures
860 in the simulations with N₂ ice deposits outside SP are slightly less than in the
861 simulation without deposits outside SP.

862 6 Discussion

863 In this paper we do not seek to reproduce precisely how the SP basin filled
864 with N₂ ice, since many parameters are unknown (e.g. the origin of the basin,
865 or the obliquity and the orbital conditions at the time it formed). In addition
866 we do not take into account the reorientation of the rotation axis (Keane et al.,
867 2016) and, last but not least, the methane and CO cycles and the presence of
868 methane and CO ices which can strongly affect the surface albedo, emissivity,
869 temperatures and the rheology of the N₂ ice (and its sublimation if CH₄-rich
870 ice layers form on the N₂ ice). Instead, we seek to evaluate if N₂ deposits
871 outside SP could have remained for a long time on Pluto and form perennial
872 deposits, and if yes, at which latitudes.

Table 1. Settings and results of the simulations performed from 30 Myrs ago to present-day. From left to right, settings are: name of the run (the runs marked by * are illustrated by Figure 14 and Figure 15), thermal inertia, N_2 ice reservoir (globally averaged), N_2 ice albedo. Results are: latitudes between which N_2 ice deposits are obtained outside SP, latitudes where the N_2 ice deposits are obtained outside SP peak, altitude of the N_2 ice deposits inside SP, altitude of N_2 ice outside SP, time needed to fill SP with N_2 ice at 95% of its final state, minimum and maximum surface pressures obtained during the last 15 Myrs

Run	Thermal inertia ($J s^{-1/2} m^{-2} K^{-1} kg m^{-2}$)	Reservoir ($kg m^{-2}$)	Albedo A_{N_2}	Latitude N_2		Peak N_2 outside SP	H_{ice} in SP (m)	H_{ice} outside SP (m)	$\tau_{95\%}^{SP}$ (Myrs)	Surface Pressure (Pa)	
				outside SP	outside SP					P_{min}	P_{max}
#Polar1*	400	200	0.7	15°N-22.5°N	18°N	18°N	-3960	330	22.45	0.0056	4.945
#Polar2	400	500	0.7	30°S-30°N	15°S	15°S	-1540	400-600	10.15	0.0166	3.977
#Polar3	400	1000	0.7	50°S-50°N	10°S	10°S	440	1000-1200	6.55	0.0234	2.371
#Polar4*	800	200	0.7	No ice	/	/	-3290	0	26.55	0.0229	2.355
#Polar5	800	500	0.7	30°S-30°N	Equator	Equator	-2110	500-750	27.05	0.0371	2.101
#Polar6	800	1000	0.7	50°S-50°N	Equator	Equator	440	1000-1200	12.30	0.0523	1.527
#Polar7	1200	200	0.7	No ice	/	/	-3290	0	35.00	0.1498	2.862
#Polar8*	1200	500	0.7	30°S-30°N	Equator	Equator	-2350	500-800	11.90	0.0513	1.393
#Polar9	1200	1000	0.7	50°S-50°N	Equator	Equator	430	1000-1200	12.50	0.0679	1.162
#Polar10	400	500	0.4	30°S-37.5°N	5°N or locally in the depressions	5°N or locally in the depressions	-1740	600-800	7.45	0.8433	88.485
#Polar11	800	500	0.4	30°S-37.5°N	Equator or locally in the depressions	Equator or locally in the depressions	-1820	600-800	7.50	1.8224	70.005
#Polar12*	1200	500	0.4	30°S-37.5°N	Equator or locally in the depressions	Equator or locally in the depressions	-1850	700-800	7.55	2.5942	62.690
#Equa1	400	200	0.7	No ice	/	/	-3290	0	19.15	0.0073	4.919
#Equa2	400	500	0.7	30°S-30°N	10°S	10°S	-1460	500-700	9.75	0.0160	4.192
#Equa3	400	1000	0.7	50°S-50°N	18°S	18°S	450	1000-1200	7.40	0.0232	2.397
#Equa4	800	200	0.7	20°S-20°N	10°S, 10°N, less ice at the equator	10°S, 10°N, less ice at the equator	-5290	300-400	7.95	0.0241	2.218
#Equa5	800	500	0.7	37.5°S-37.5°N	Equator	Equator	-2030	600-700	27.85	0.0320	1.975
#Equa6	800	1000	0.7	50°S-50°N	Equator	Equator	460	1000-1200	12.25	0.0527	1.536
#Equa7	1200	200	0.7	20°S-20°N	10°S, 10°N, less ice at the equator	10°S, 10°N, less ice at the equator	-5340	300-400	7.70	0.0375	1.381
#Equa8	1200	500	0.7	30°S-30°N	Equator	Equator	-2160	700-800	30.35	0.0485	1.448
#Equa9	1200	1000	0.7	50°S-50°N	Equator	Equator	440	1000-1200	12.20	0.0704	1.184
#Equa10	400	500	0.4	30°S-37.5°N	5°N or locally in the depressions	5°N or locally in the depressions	-1740	600-800	9.65	0.8430	88.483
#Equa11	800	500	0.4	37.5°S-45°N	Equator or locally in the depressions	Equator or locally in the depressions	-1820	600-800	9.40	1.8220	70.006
#Equa12	1200	500	0.4	30°S-37.5°N	Equator or locally in the depressions	Equator or locally in the depressions	-1850	700-800	8.10	2.5915	62.693
#Glob1*	400	200	0.7	No ice	/	/	-3290	0	17.15	0.0073	4.754
#Glob2	400	500	0.7	30°S-30°N	10°S	10°S	-1500	500-650	11.45	0.0160	4.147
#Glob3	400	1000	0.7	50°S-50°N	18°S	18°S	470	1000-1200	6.65	0.0222	2.391
#Glob4*	800	200	0.7	20°S-20°N	10°S, 10°N, less ice at the equator	10°S, 10°N, less ice at the equator	-5200	250-400	6.10	0.0258	2.190
#Glob5	800	500	0.7	30°S-30°N	Equator	Equator	-3040	650-750	25.05	0.0320	1.932
#Glob6	800	1000	0.7	50°S-50°N	Equator	Equator	450	1200	12.00	0.0533	1.532
#Glob7*	1200	200	0.7	20°S-20°N	10°S, 10°N, less ice at the equator	10°S, 10°N, less ice at the equator	-5010	200-350	7.40	0.0372	1.373
#Glob8	1200	500	0.7	30°S-30°N	Equator	Equator	-2250	100-800	26.40	0.0461	1.373
#Glob9	1200	1000	0.7	50°S-50°N	Equator	Equator	430	1200	12.30	0.0669	1.370
#Glob10	400	500	0.4	30°S-37.5°N	5°N or locally in the depressions	5°N or locally in the depressions	-1740	600-800	7.90	0.8429	88.487
#Glob11	800	500	0.4	30°S-37.5°N	Equator or locally in the depressions	Equator or locally in the depressions	-1830	600-800	7.90	1.8219	70.011
#Glob12*	1200	500	0.4	30°S-30°N	Equator or locally in the depressions	Equator or locally in the depressions	-1860	700-800	7.95	2.5917	62.722

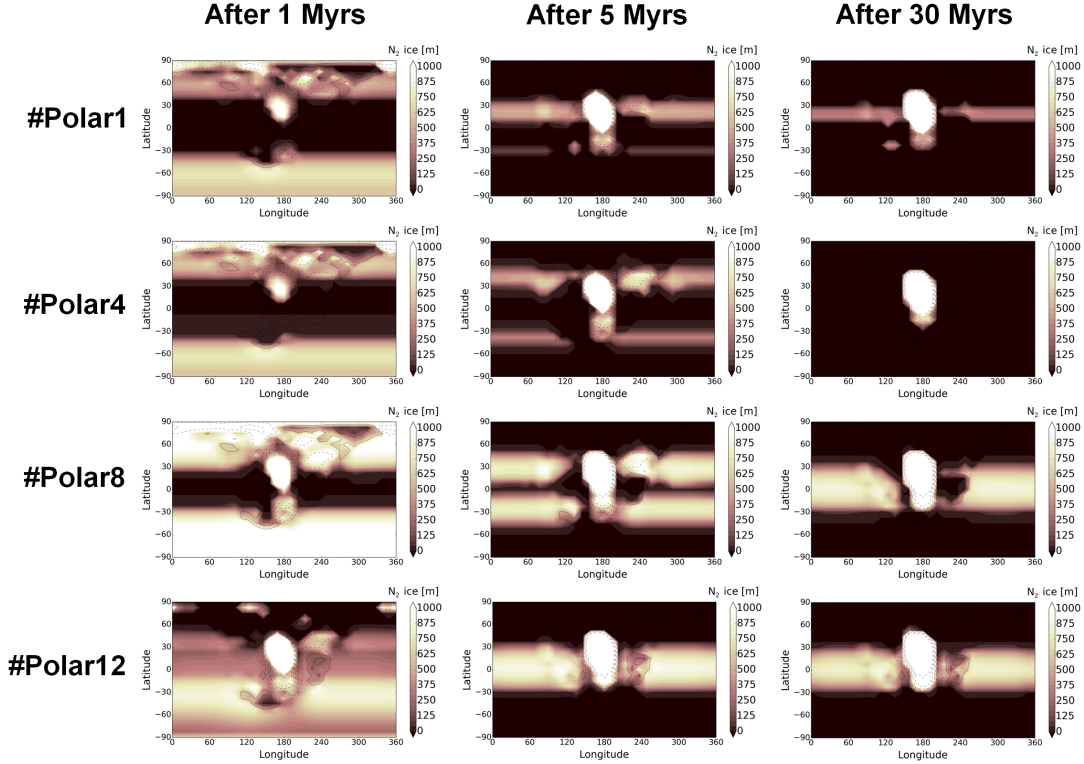


Fig. 14. Maps of N_2 ice distribution on Pluto (m) for simulations starting 30 Myrs ago with a polar reservoir (#Polar1, #Polar4, #Polar8, #Polar12). Results are shown after 1 Myrs (left panel), 5 Myrs (middle panel) and 30 Myrs (right panel).

873 In our previous paper [Bertrand and Forget \(2016\)](#), we showed that any condensed N_2 ice on Pluto's surface tends to end inside the Sputnik Planitia
874 basin. Here, we reproduced similar simulations by taking into account large
875 reservoirs of N_2 ice able to sublime, condense and flow over several Myrs
876 through the changes of obliquity and orbital parameters of Pluto. We found
877 again that any large N_2 ice deposits outside SP would accumulate in SP and
878 fill the basin with several kilometres of ice. However, this would take several
879 tens of Myrs during which transient states exist for the deposits. Indeed, as-
880 suming that the basin formed initially without N_2 ice inside, our results show
881 that large deposits of several hundreds of meters of N_2 ice, placed at the poles,
882 are not stable there, and would inevitably accumulate first at mid-latitudes
883 over an entire latitudinal band after few Myrs, and then, in some cases, in
884 more equatorial regions after tens of Myrs. We estimate that the basin would
885 be filled up by several kilometers of ice in few Myrs. In the mid-latitude and
886 equatorial regions, the deposits are relatively stable and may remain there
887 during 10-100s of Myrs before to end in Sputnik Planitia, depending on the
888 thermal inertia, the albedo of the ice, the local topography, etc. These results
889 raise discussions about the impact of such glaciers outside SP on the geology
890 of Pluto and on the surface pressures encountered in Pluto's past.
891

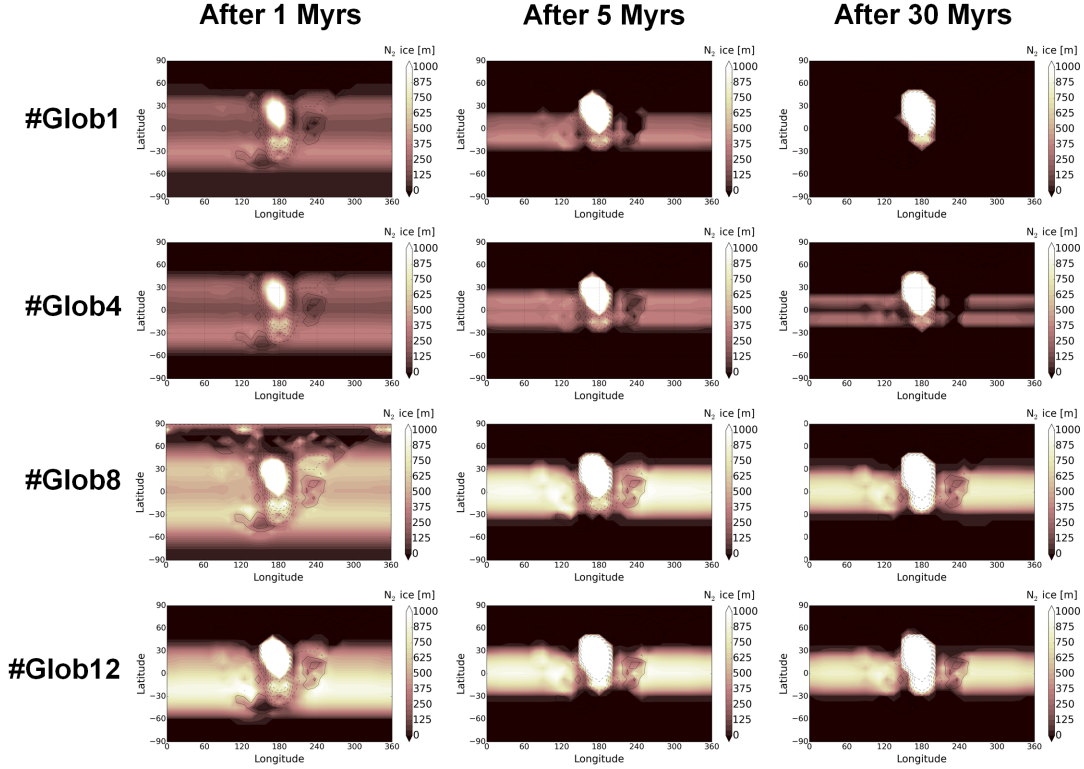


Fig. 15. Maps of N_2 ice distribution on Pluto (m) for simulations starting 30 Myrs ago with a global reservoir (#Glob1, #Glob4, #Glob8, #Glob12). Results are shown after 1 Myrs (left panel), 5 Myrs (middle panel) and 30 Myrs (right panel).

892 First, parts of the equatorial regions of Pluto (and in particular in Cthulhu
 893 region) are covered by numerous geologically old craters which do not seem
 894 particularly eroded by ancient deposition of N_2 ice. Is it possible that nitrogen
 895 ice accumulated in this region and did not eroded the bedrock? We believe that
 896 cold/dry based glaciation has a good erosive ability on Pluto and therefore
 897 that it unlikely that hundreds of meters of ice accumulated in this region in
 898 the past. Although the erosive properties of nitrogen ice at these temperatures
 899 are unknown (nothing has been published on this issue yet), we are guided
 900 (1) by the erosive mechanisms that exist on the Earth, where dry/cold based
 901 glaciation has been shown to be possible (Atkins et al., 2002), although it is
 902 difficult to show if it is efficient or not under Pluto's conditions, and (2) by
 903 the fact that the water ice bedrock has been strongly eroded around Sputnik
 904 Planitia, possibly involving dry glaciation (since on the edges of the ice cap,
 905 the ice layer is thin and dry basal flow should dominate).

906 In addition, if large N_2 deposits existed outside SP, they may not have been
 907 large enough to flow toward the equatorial regions (like in our simulations
 908 started with a global reservoir of ice less than 200 m). Or, the equatorial
 909 regions may have been already warmer than the higher latitudes, due to a low
 910 thermal inertia (less than 800 SI) or due to albedo gradients (dark tholins at

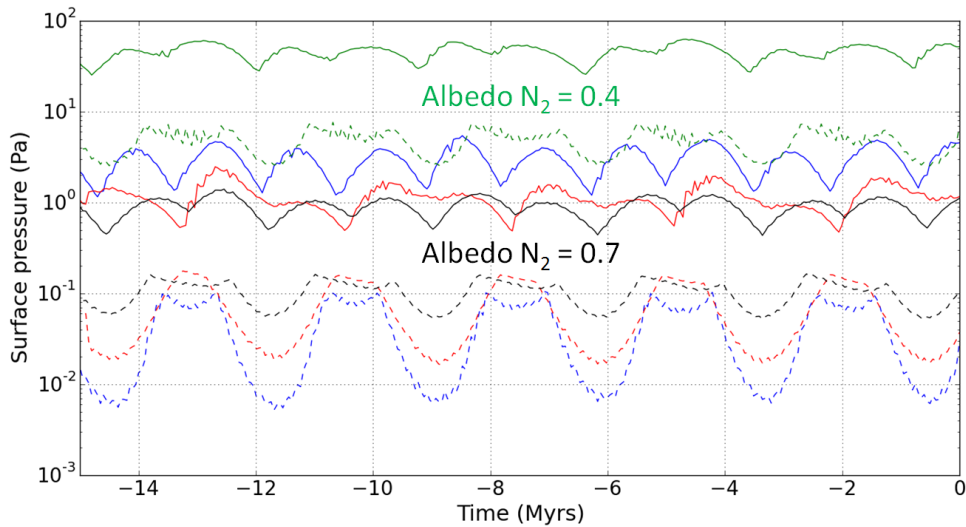


Fig. 16. Evolution of maximum (solid lines) and minimum (dashed lines) annual surface pressure over the last 15 Myrs for simulations starting with a polar reservoir: #Polar1 (blue), #Polar4 (red), #Polar8 (black), #Polar12 (green). The present-day maximum surface pressure is ~ 1.1 Pa (Stern et al., 2015; Gladstone et al., 2016; Hinson et al., 2017).

911 the equator and bright methane ice at higher latitudes, see also (Earle et al.,
 912 2018)).

913 In some of our simulations, relatively stable deposits of N_2 ice are obtained
 914 outside SP at higher latitudes, without any ice at the equator. This is for
 915 example the case for simulations with a reservoir of 200 m, such as #Polar1,
 916 #Polar4, where the ice does not flow toward the equator but forms latitudinal
 917 bands between 25°S - 45°S and 25°N - 45°N . Interestingly, several surface fea-
 918 tures on Pluto have been interpreted as evidence for past liquid flow, and they
 919 are all observed around the latitudes ± 30 - 60° (Stern et al., 2017). These lat-
 920 itudes correspond to the regions where ice accumulates in our model (outside
 921 SP), first as a transient state (thick glaciers over latitudinal bands) and then
 922 as a final state at mid-latitudes around 10 - 30°N (swallower glaciers because
 923 most of the ice is trapped inside SP), in particular if a low TI and N_2 reservoir
 924 are considered. It has been suggested that epochs with higher atmospheric
 925 pressure occurred in Pluto's geologic past and enabled the nitrogen ice to
 926 be much warmer, perhaps even to turn to liquid, and to flow on the surface
 927 leading to the formation of these features (Stern et al., 2017). However, here
 928 our simulations demonstrate that surface pressures higher than 100 Pa are
 929 unlikely to have occurred in Pluto's past, because the large reservoirs of ni-
 930 trogen ice are located in the cold and stable equatorial regions and because
 931 the relatively high thermal inertia and albedo of the ice limit the sublimation
 932 and condensation fluxes. We even found that pressures are the lowest during

933 the high obliquity periods, because N_2 ice is never stable at the poles at the
934 scale of the astronomical cycles and therefore not available for intense polar
935 sublimation during these periods. Note that in 2015, which corresponds to
936 northern spring on Pluto, the observed surface of the north polar regions of
937 Pluto was free of N_2 ice (Schmitt et al., 2017; Grundy et al., 2016). There will
938 be no N_2 ice available at the pole to sublimate during summer and increase the
939 pressure. In addition, in our simulations, the maximum surface pressures raise
940 up to ~ 100 Pa if the ice albedo is set to 0.4, which is a very low value for an
941 ice as mobile as N_2 on Pluto. Therefore we propose that the paleoliquids - and
942 other terrains thought to have been shaped and altered by liquid flows - are
943 the results of past liquid flows which occurred at the base of massive nitrogen
944 glaciers (basal flow), which accumulated at the mid-latitudes because they are
945 the coldest points on Pluto in average (an effect depending on thermal inertia,
946 as shown by Figure 4). These glaciers may have remained at these latitudes
947 for millions of years before they disappear, the ice ending inside SP.

948 What would trigger the formation of perennial N_2 ice deposits on Pluto outside
949 SP ? Since the astronomical cycles of Pluto are relatively stable, we can make
950 the hypothesis that the perennial ice deposits on present-day Pluto reached
951 a steady-state. In that case the entire reservoir of N_2 ice should be trapped
952 in SP, as suggested by our model results showing that N_2 ice deposits out-
953 side SP still accumulates in SP after 30 Myrs, losing about 10 m per Myrs.
954 However, other processes could help to maintain perennial N_2 ice deposits and
955 feed Pluto's surface with N_2 ice outside SP, such as cryovolcanism or bright
956 methane deposits enabling N_2 ice to condense on it (see below).

957 What is the nature (seasonal or perennial) of the different reservoirs of N_2 ice
958 observed in 2015 by New Horizons? How did they form? Observationally, it
959 is difficult to know because we do not know the thickness of these reservoirs,
960 although they do not look like several hundreds of meters deep. The amounts
961 of diluted CH_4 and CO vary in these deposits, which is indicative of volatile
962 evolution processes (Protopapa et al., 2017; Schmitt et al., 2017). In Bertrand
963 and Forget (2016), we show that regions covered by dark tholins do not favour
964 N_2 condensation on it, while surfaces covered by bright methane frost do. In
965 fact, the latitudinal band of nitrogen observed by New Horizons between $30^\circ N$ -
966 $60^\circ N$ has been reproduced by the volatile transport model when high methane
967 albedo (> 0.65) were considered (see Figure 3 in Bertrand and Forget (2016)).
968 In this scenario, the latitudinal band of N_2 ice is seasonal since it forms on
969 the cold methane polar frost in winter and sublimates during spring from the
970 pole. However, if the thermal inertia is lower than the 800 SI assumed in this
971 scenario, then our results suggest that the ice may be more stable at these
972 latitudes and the latitudinal band of N_2 ice may be perennial, continuously fed
973 by seasonal frosts. In other words, bright methane frosts may have helped to
974 maintain the latitudinal bands of massive N_2 deposits as a perennial reservoir
975 (e.g. as the one obtained in the case #Polar1 or #Polar4 in Figure 14). Simi-

976 lar arguments apply for the region East of Tombaugh region: bright methane
977 deposits coupled with relatively low-altitude terrains may favour the accumu-
978 lation of N₂ ice there, which can remain relatively stable over time, especially
979 if the TI is high and thus favouring more stable deposits close to the equator.
980 In this paper, thin seasonal polar nitrogen frosts have been obtained in most of
981 the simulations. Although we noted that a lower thermal inertia favour thicker
982 deposits at the poles, simulations taking into account bright methane deposits
983 are necessary to fully investigate the evolution of polar frosts, and will be the
984 topic of future studies.

985 Finally, as predicted by the model, N₂ ice is more stable in the depressions
986 than in higher terrains. In fact, a limited number of spots of N₂-rich ice have
987 been observed in the dark equatorial region of Cthulhu, in particular in the
988 Oort and Edgeworth craters (Schmitt et al., 2017). Note that preferential de-
989 position of N₂ ice at the latitudes $\pm 10^\circ$ or $\pm 20^\circ$ (with the equator free of
990 ice) would be consistent with our results obtained with TI between 400-800
991 SI showing latitudinal bands of stable deposits at these latitudes (#Polar1,
992 #Equa4, #Equa7, #Glob4, #Glob7). The lack of data makes it difficult to as-
993 sess, and low-resolution data in the sub-Charon hemisphere is currently under
994 processing and analysis. Ground-based telescopic observations rule out the
995 presence of large expanses of N₂ ice on the sub-Charon hemisphere, but not
996 the presence of small patches, which are impossible to see from the ground
997 (Grundy et al., 2013).

998 7 Conclusions

999 The Pluto volatile transport model has been used to investigate the cycles of
1000 nitrogen on Pluto over diurnal, seasonal and astronomical timescales, taking
1001 into account the changes of obliquity, longitude of perihelion and eccentricity
1002 and the flow of N₂ ice and the changes of topography induced (following the
1003 rheology and glacial flow equations as described in Umurhan et al. (2017)).

1004 Our first conclusion is that Pluto's climate is impacted by the universal Mi-
1005 lankovitch mechanism, as the Earth, Mars and Titan. The changes of obliquity
1006 and orbital parameters lead to differences of surface temperatures between
1007 poles and equator, and asymmetries in the season. We described in this paper
1008 how the most volatile ice of Pluto, N₂ ice, is impacted by these changes over
1009 time.

1010 We first focused on the nitrogen cycles within the Sputnik Planitia basin, con-
1011 sidering that it is the only known perennial reservoir of nitrogen ice on Pluto.
1012 The results suggest that Sputnik Planitia has a complex history, related to
1013 sublimation, condensation, and glacial flow involved at different timescales.

1014 High obliquity periods induce intense polar summers and thus intense subli-
1015 mation rates in the northern part of the ice sheet. During the last 2 million
1016 years, this part would have lost up to 1 km of ice by sublimation. On the
1017 other hand, low obliquity periods favour sublimation in the center of Sputnik
1018 Planitia and condensation at the north and south extremities, of up to 300
1019 m of ice in 1 million years. The glacial flow activity (ice flowing toward the
1020 center of Sputnik Planitia) observed at the eastern edge of the ice sheet can
1021 thus be related to the intense condensation of nitrogen ice which occurred at
1022 these latitudes during the past 2 million years, while the methane-enriched
1023 N₂ ice dark plains are linked to the intense sublimation which occurred north
1024 of Sputnik Planitia during the same period. The deep pits observed in the
1025 south of Sputnik Planitia may have started to form 100,000 years ago, when
1026 the southern latitudes of the ice sheet entered a net sublimation-dominated
1027 regime. The bright plains in the center of Sputnik Planitia can be explained
1028 by the current seasonal accumulation of ice there. Finally, the depressions ob-
1029 served north and south of the ice sheet, as well as the strong erosion of the
1030 Al-Idrisi Montes, are consistent with the simulated glacial activity of Sputnik
1031 Planitia, with continuous variation of elevations at the edges of the ice sheet
1032 up to 300 m every obliquity cycle. The results also show that in current epoch,
1033 the ice sheet is close to its minimal extension (in the model in current epoch
1034 the center of SP has a higher elevation than the northern and southern edges
1035 of SP), which is consistent with the observations showing evidences of strong
1036 erosion further north (Al-Idrisi) and south (West and East of Tenzing Montes)
1037 of the ice sheet.

1038 We also explored the stability of N₂ ice deposits outside Sputnik Planitia. Our
1039 simulations show that nitrogen ice tends to end inside Sputnik Planitia but
1040 if large deposits are formed outside SP, they should accumulate and persist
1041 in the mid-latitude and equatorial regions for several tens of million years.
1042 In particular, N₂ ice accumulates in the depressions. For instance, in most of
1043 the simulations involving N₂ ice in the equatorial regions, no N₂ ice has been
1044 obtained in the Tartarus Dorsa region, featuring the high altitude bladed
1045 terrains. The latitudes where N₂ ice accumulates depends on the seasonal
1046 thermal inertia (the higher it is, the more equatorial are the deposits), the ice
1047 albedo, the initial distribution and probably other parameters not taken into
1048 account in this paper such as the methane ice distribution. Our simulations
1049 support the case of low to medium thermal inertia (400-800 SI) for several
1050 reasons. It enables to reproduce the evolution of pressure since 1988 ([Bertrand
1051 and Forget, 2016](#)). In some cases, it enables formation of perennial deposits
1052 at mid-latitudes but not at the equator, which remains free of volatile ice.

1053 Geomorphological evidences of past liquid flows have been observed at Pluto's
1054 surface at the same mid-latitude. Therefore we suggest that they formed by
1055 liquid nitrogen flows at the base of ancient thick nitrogen glaciers instead
1056 of formed by liquid nitrogen flows directly at Pluto's surface during higher

1057 pressure epochs in Plutos geologic past, as suggested by [Stern et al. \(2017\)](#).
1058 This is reinforced by our results showing that the minimum and maximum
1059 surface pressures obtained in our simulations always remain in the range of
1060 milli-Pascals and tens of Pascals, respectively. Therefore surface temperatures
1061 never reach the triple point of nitrogen. It is not possible to reach higher
1062 pressures in Pluto's past with our model because the sublimation-condensation
1063 flux are limited by the medium to high thermal inertia and the relatively bright
1064 albedo assumed for the N₂ ice (> 0.4).

1065 Finally, the cycle of nitrogen ice on Pluto can be impacted by other processes,
1066 not taken into account in the simulations of this paper. In particular, methane
1067 ice is known to play a complex role since it can cold trap nitrogen ice if its
1068 albedo is high enough ([Bertrand and Forget, 2016](#); [Earle et al., 2018](#)), which
1069 could explain why many patches of nitrogen ice are observed outside Sputnik
1070 Planitia. A study taking into account both cycles of methane and nitrogen,
1071 over all timescales, is in preparation and should help to better understand how
1072 these ices evolve on Pluto.

1073 **References**

- 1074 O. Aharonson, A. G. Hayes, J. I. Lunine, R. D. Lorenz, M. D. Allison, and
1075 C. Elachi. An asymmetric distribution of lakes on Titan as a possible con-
1076 sequence of orbital forcing. *Nature Geoscience*, 2:851–854, December 2009.
1077 doi: 10.1038/ngeo698.
- 1078 C. B. Atkins, P. J. Barrett, and S. R. Hicock. Cold glaciers erode and deposit:
1079 Evidence from Allan Hills, Antarctica. *Geology*, 30:659, July 2002. doi:
1080 10.1130/0091-7613(2002)030<0659:CGEADE>2.0.CO;2.
- 1081 T. Bertrand and F. Forget. Observed glacier and volatile distribution on Pluto
1082 from atmospheretopography processes. *Nature*, 987, December 2016. doi:
1083 10.1038/nature19337.
- 1084 R. P. Binzel, A. M. Earle, M. W. Buie, L. A. Young, S. A. Stern, C. B. Olkin,
1085 K. Ennico, J. M. Moore, W. Grundy, H. A. Weaver, C. M. Lisse, and T. R.
1086 Lauer. Climate zones on Pluto and Charon. *Icarus*, 287:30–36, May 2017.
1087 doi: 10.1016/j.icarus.2016.07.023.
- 1088 M. W. Buie, D. J. Tholen, and L. H. Wasserman. Separate Lightcurves of
1089 Pluto and Charon. *Icarus*, 125:233–244, February 1997. doi: 10.1006/icar.
1090 1996.5624.
- 1091 B. J. Buratti, J. D. Hofgartner, M. D. Hicks, H. A. Weaver, S. A. Stern,
1092 T. Momary, J. A. Mosher, R. A. Beyer, A. J. Verbiscer, A. M. Zangari,
1093 L. A. Young, C. M. Lisse, K. Singer, A. Cheng, W. Grundy, K. Ennico, and
1094 C. B. Olkin. Global albedos of Pluto and Charon from LORRI New Horizons
1095 observations. *Icarus*, 287:207–217, May 2017. doi: 10.1016/j.icarus.2016.11.
1096 012.
- 1097 A. R. Dobrovolskis, S. J. Peale, and A. W. Harris. *Dynamics of the Pluto-*
1098 *Charon Binary*. In: S.A. Stern, D.J. Tholen (Eds.), *Pluto and Charon*,
1099 *University of Arizona Press, Tucson, 159-190*. 1997.
- 1100 W. B. Durham, O. Prieto-Ballesteros, D. L. Goldsby, and J. S. Kargel. Rheo-
1101 logical and Thermal Properties of Icy Materials. *Space Sci. Rev.*, 153:
1102 273–298, June 2010. doi: 10.1007/s11214-009-9619-1.
- 1103 A. M. Earle, R. P. Binzel, L. A. Young, S. A. Stern, K. Ennico, W. Grundy,
1104 C. B. Olkin, and H. A. Weaver. Long-term surface temperature modeling
1105 of Pluto. *Icarus*, 287:37–46, May 2017. doi: 10.1016/j.icarus.2016.09.036.
- 1106 A. M. Earle, R. P. Binzel, L. A. Young, S. A. Stern, K. Ennico, W. Grundy,
1107 C. B. Olkin, H. A. Weaver, and New Horizons Surface Composition Theme.
1108 Albedo matters: Understanding runaway albedo variations on Pluto. *Icarus*,
1109 303:1–9, March 2018. doi: 10.1016/j.icarus.2017.12.015.
- 1110 F. Forget, R. M. Haberle, F. Montmessin, B. Levrard, and J. W. Head. For-
1111 mation of Glaciers on Mars by Atmospheric Precipitation at High Obliquity.
1112 *Science*, 311:368–371, January 2006. doi: 10.1126/science.1120335.
- 1113 F. Forget, T. Bertrand, M. Vangvichith, J. Leconte, E. Millour, and E. Lel-
1114 louch. A post-new horizons global climate model of Pluto including the N₂,
1115 CH₄ and CO cycles. *Icarus*, 287:54–71, May 2017. doi: 10.1016/j.icarus.
1116 2016.11.038.

- 1117 G. R. Gladstone, S. A. Stern, K. Ennico, C. B. Olkin, H. A. Weaver, L. A.
1118 Young, M. E. Summers, D. F. Strobel, D. P. Hinson, J. A. Kammer, A. H.
1119 Parker, A. J. Steffl, I. R. Linscott, J. W. Parker, A. F. Cheng, D. C. Slater,
1120 M. H. Versteeg, T. K. Greathouse, K. D. Retherford, H. Throop, N. J. Cun-
1121 ningham, W. W. Woods, K. N. Singer, C. C. C. Tsang, E. Schindhelm,
1122 C. M. Lisse, M. L. Wong, Y. L. Yung, X. Zhu, W. Curdt, P. Lavvas, E. F.
1123 Young, G. L. Tyler, F. Bagenal, W. M. Grundy, W. B. McKinnon, J. M.
1124 Moore, J. R. Spencer, T. Andert, J. Andrews, M. Banks, B. Bauer, J. Bau-
1125 man, O. S. Barnouin, P. Bedini, K. Beisser, R. A. Beyer, S. Bhaskaran,
1126 R. P. Binzel, E. Birath, M. Bird, D. J. Bogan, A. Bowman, V. J. Bray,
1127 M. Brozovic, C. Bryan, M. R. Buckley, M. W. Buie, B. J. Buratti, S. S.
1128 Bushman, A. Calloway, B. Carcich, S. Conard, C. A. Conrad, J. C. Cook,
1129 D. P. Cruikshank, O. S. Custodio, C. M. D. Ore, C. Deboy, Z. J. B. Dischner,
1130 P. Dumont, A. M. Earle, H. A. Elliott, J. Ercol, C. M. Ernst, T. Finley, S. H.
1131 Flanigan, G. Fountain, M. J. Freeze, J. L. Green, Y. Guo, M. Hahn, D. P.
1132 Hamilton, S. A. Hamilton, J. Hanley, A. Harch, H. M. Hart, C. B. Hersman,
1133 A. Hill, M. E. Hill, M. E. Holdridge, M. Horanyi, A. D. Howard, C. J. A.
1134 Howett, C. Jackman, R. A. Jacobson, D. E. Jennings, H. K. Kang, D. E.
1135 Kaufmann, P. Kollmann, S. M. Krimigis, D. Kusnierkiewicz, T. R. Lauer,
1136 J. E. Lee, K. L. Lindstrom, A. W. Lunsford, V. A. Mallder, N. Martin, D. J.
1137 McComas, R. L. McNutt, D. Mehoke, T. Mehoke, E. D. Melin, M. Mutchler,
1138 D. Nelson, F. Nimmo, J. I. Nunez, A. Ocampo, W. M. Owen, M. Paetzold,
1139 B. Page, F. Pelletier, J. Peterson, N. Pinkine, M. Piquette, S. B. Porter,
1140 S. Protopapa, J. Redfern, H. J. Reitsema, D. C. Reuter, J. H. Roberts, S. J.
1141 Robbins, G. Rogers, D. Rose, K. Runyon, M. G. Ryschkewitsch, P. Schenk,
1142 B. Sepan, M. R. Showalter, M. Soluri, D. Stanbridge, T. Stryk, J. R. Szalay,
1143 M. Tapley, A. Taylor, H. Taylor, O. M. Umurhan, A. J. Verbiscer, M. H.
1144 Versteeg, M. Vincent, R. Webbert, S. Weidner, G. E. Weigle, O. L. White,
1145 K. Whittenburg, B. G. Williams, K. Williams, S. Williams, A. M. Zangari,
1146 and E. Zirnstein. The atmosphere of Pluto as observed by New Horizons.
1147 *Science*, 351:aad8866, March 2016. doi: 10.1126/science.aad8866.
- 1148 W. M. Grundy, C. B. Olkin, L. A. Young, M. W. Buie, and E. F. Young.
1149 Near-infrared spectral monitoring of Pluto’s ices: Spatial distribution and
1150 secular evolution. *Icarus*, 223:710–721, April 2013. doi: 10.1016/j.icarus.
1151 2013.01.019.
- 1152 W. M. Grundy, R. P. Binzel, B. J. Buratti, J. C. Cook, D. P. Cruikshank,
1153 C. M. Dalle Ore, A. M. Earle, K. Ennico, C. J. A. Howett, A. W. Lunsford,
1154 C. B. Olkin, A. H. Parker, S. Philippe, S. Protopapa, E. Quirico, D. C.
1155 Reuter, B. Schmitt, K. N. Singer, A. J. Verbiscer, R. A. Beyer, M. W. Buie,
1156 A. F. Cheng, D. E. Jennings, I. R. Linscott, J. W. Parker, P. M. Schenk,
1157 J. R. Spencer, J. A. Stansberry, S. A. Stern, H. B. Throop, C. C. C. Tsang,
1158 H. A. Weaver, G. E. Weigle, and L. A. Young. Surface compositions across
1159 Pluto and Charon. *Science*, 351:aad9189, March 2016. doi: 10.1126/science.
1160 aad9189.
- 1161 D. P. Hamilton, S. A. Stern, J. M. Moore, L. A. Young, R. P. Binzel, M. W.

- 1162 Buie, B. J. Buratti, A. F. Cheng, K. Ennico, W. M. Grundy, I. R. Linscott,
1163 W. B. McKinnon, C. B. Olkin, H. J. Reitsema, D. C. Reuter, P. Schenk,
1164 M. R. Showalter, J. R. Spencer, G. L. Tyler, and H. A. Weaver. The rapid
1165 formation of Sputnik Planitia early in Pluto’s history. *Nature*, 540:97–99,
1166 December 2016. doi: 10.1038/nature20586.
- 1167 D. P. Hinson, I. R. Linscott, L. A. Young, G. L. Tyler, S. A. Stern, R. A. Beyer,
1168 M. K. Bird, K. Ennico, G. R. Gladstone, C. B. Olkin, M. Pätzold, P. M.
1169 Schenk, D. F. Strobel, M. E. Summers, H. A. Weaver, and W. W. Woods.
1170 Radio occultation measurements of Pluto’s neutral atmosphere with New
1171 Horizons. *Icarus*, 290:96–111, July 2017. doi: 10.1016/j.icarus.2017.02.031.
- 1172 A. D. Howard, J. M. Moore, O. M. Umurhan, O. L. White, R. S. Anderson,
1173 W. B. McKinnon, J. R. Spencer, P. M. Schenk, R. A. Beyer, S. A. Stern,
1174 K. Ennico, C. B. Olkin, H. A. Weaver, and L. A. Young. Present and past
1175 glaciation on Pluto. *Icarus*, 287:287–300, May 2017. doi: 10.1016/j.icarus.
1176 2016.07.006.
- 1177 J. T. Keane, I. Matsuyama, S. Kamata, and J. K. Steckloff. Reorientation and
1178 faulting of Pluto due to volatile loading within Sputnik Planitia. *Nature*,
1179 540:90–93, December 2016. doi: 10.1038/nature20120.
- 1180 E. Lellouch, J. Stansberry, J. Emery, W. Grundy, and D. P. Cruikshank. Ther-
1181 mal properties of Pluto’s and Charon’s surfaces from Spitzer observations.
1182 *Icarus*, 214:701–716, August 2011. doi: 10.1016/j.icarus.2011.05.035.
- 1183 B. Levrard, F. Forget, F. Montmessin, and J. Laskar. Recent formation and
1184 evolution of northern Martian polar layered deposits as inferred from a
1185 Global Climate Model. *Journal of Geophysical Research (Planets)*, 112
1186 (E11):E06012, 2007. doi: 10.1029/2006JE002772.
- 1187 J.-B. Madeleine, F. Forget, J. W. Head, B. Levrard, F. Montmessin, and
1188 E. Millour. Amazonian northern mid-latitude glaciation on Mars: A pro-
1189 posed climate scenario. *Icarus*, 203:390–405, 2009. doi: 10.1016/j.icarus.
1190 2009.04.037.
- 1191 W. B. McKinnon, F. Nimmo, T. Wong, P. M. Schenk, O. L. White, J. H.
1192 Roberts, J. M. Moore, J. R. Spencer, A. D. Howard, O. M. Umurhan, S. A.
1193 Stern, H. A. Weaver, C. B. Olkin, L. A. Young, K. E. Smith, R. Beyer,
1194 M. Buie, B. Buratti, A. Cheng, D. Cruikshank, C. Dalle Ore, R. Glad-
1195 stone, W. Grundy, T. Lauer, I. Linscott, J. Parker, S. Porter, H. Reit-
1196 sema, D. Reuter, S. Robbins, M. Showalter, K. Singer, D. Strobel, M. Sum-
1197 mers, L. Tyler, M. Banks, O. Barnouin, V. Bray, B. Carcich, A. Chaikin,
1198 C. Chavez, C. Conrad, D. Hamilton, C. Howett, J. Hofgartner, J. Kammer,
1199 C. Lisse, A. Marcotte, A. Parker, K. Retherford, M. Saina, K. Runyon,
1200 E. Schindhelm, J. Stansberry, A. Steffl, T. Stryk, H. Throop, C. Tsang,
1201 A. Verbiscer, H. Winters, A. Zangari, and G. a. I. T. T. New Horizons
1202 Geology. Convection in a volatile nitrogen-ice-rich layer drives Pluto’s geo-
1203 logical vigour. *Nature*, 534:82–85, June 2016. doi: 10.1038/nature18289.
- 1204 M. A. Mischna, M. I. Richardson, R. J. Wilson, and D. J. McCleese. On the
1205 orbital forcing of Martian water and CO₂ cycles: A general circulation model
1206 study with simplified volatile schemes. *Journal of Geophysical Research*

- 1207 (*Planets*), pages 16–1, 2003.
- 1208 J. M. Moore, W. B. McKinnon, J. R. Spencer, A. D. Howard, P. M. Schenk,
 1209 R. A. Beyer, F. Nimmo, K. N. Singer, O. M. Umurhan, O. L. White, S. A.
 1210 Stern, K. Ennico, C. B. Olkin, H. A. Weaver, L. A. Young, R. P. Binzel,
 1211 M. W. Buie, B. J. Buratti, A. F. Cheng, D. P. Cruikshank, W. M. Grundy,
 1212 I. R. Linscott, H. J. Reitsema, D. C. Reuter, M. R. Showalter, V. J. Bray,
 1213 C. L. Chavez, C. J. A. Howett, T. R. Lauer, C. M. Lisse, A. H. Parker, S. B.
 1214 Porter, S. J. Robbins, K. Runyon, T. Stryk, H. B. Throop, C. C. C. Tsang,
 1215 A. J. Verbiscer, A. M. Zangari, A. L. Chaikin, D. E. Wilhelms, F. Bagenal,
 1216 G. R. Gladstone, T. Andert, J. Andrews, M. Banks, B. Bauer, J. Bauman,
 1217 O. S. Barnouin, P. Bedini, K. Beisser, S. Bhaskaran, E. Birath, M. Bird,
 1218 D. J. Bogan, A. Bowman, M. Brozovic, C. Bryan, M. R. Buckley, S. S.
 1219 Bushman, A. Calloway, B. Carcich, S. Conard, C. A. Conrad, J. C. Cook,
 1220 O. S. Custodio, C. M. D. Ore, C. Deboy, Z. J. B. Dischner, P. Dumont,
 1221 A. M. Earle, H. A. Elliott, J. Ercol, C. M. Ernst, T. Finley, S. H. Flanigan,
 1222 G. Fountain, M. J. Freeze, T. Greathouse, J. L. Green, Y. Guo, M. Hahn,
 1223 D. P. Hamilton, S. A. Hamilton, J. Hanley, A. Harch, H. M. Hart, C. B.
 1224 Hersman, A. Hill, M. E. Hill, D. P. Hinson, M. E. Holdridge, M. Horanyi,
 1225 C. Jackman, R. A. Jacobson, D. E. Jennings, J. A. Kammer, H. K. Kang,
 1226 D. E. Kaufmann, P. Kollmann, S. M. Krimigis, D. Kusnierkiewicz, J. E.
 1227 Lee, K. L. Lindstrom, A. W. Lunsford, V. A. Mallder, N. Martin, D. J. Mc-
 1228 Comas, R. L. McNutt, D. Mehoke, T. Mehoke, E. D. Melin, M. Mutchler,
 1229 D. Nelson, J. I. Nunez, A. Ocampo, W. M. Owen, M. Paetzold, B. Page,
 1230 J. W. Parker, F. Pelletier, J. Peterson, N. Pinkine, M. Piquette, S. Pro-
 1231 topapa, J. Redfern, J. H. Roberts, G. Rogers, D. Rose, K. D. Rether-
 1232 ford, M. G. Ryschkewitsch, E. Schindhelm, B. Sepan, M. Soluri, D. Stan-
 1233 bridge, A. J. Steffl, D. F. Strobel, M. E. Summers, J. R. Szalay, M. Tapley,
 1234 A. Taylor, H. Taylor, G. L. Tyler, M. H. Versteeg, M. Vincent, R. Webbert,
 1235 S. Weidner, G. E. Weigle, K. Whittenburg, B. G. Williams, K. Williams,
 1236 S. Williams, W. W. Woods, and E. Zirnstein. The geology of Pluto and
 1237 Charon through the eyes of New Horizons. *Science*, 351:1284–1293, March
 1238 2016. doi: 10.1126/science.aad7055.
- 1239 J. M. Moore, A. D. Howard, O. M. Umurhan, O. L. White, P. M. Schenk,
 1240 R. A. Beyer, W. B. McKinnon, J. R. Spencer, W. M. Grundy, T. R. Lauer,
 1241 F. Nimmo, L. A. Young, S. A. Stern, H. A. Weaver, C. B. Olkin, and K. En-
 1242 nico. Sublimation as a landform-shaping process on Pluto. *Icarus*, 287:
 1243 320–333, May 2017. doi: 10.1016/j.icarus.2016.08.025.
- 1244 S. Protopapa, W. M. Grundy, D. C. Reuter, D. P. Hamilton, C. M. Dalle Ore,
 1245 J. C. Cook, D. P. Cruikshank, B. Schmitt, S. Philippe, E. Quirico, R. P.
 1246 Binzel, A. M. Earle, K. Ennico, C. J. A. Howett, A. W. Lunsford, C. B.
 1247 Olkin, A. Parker, K. N. Singer, A. Stern, A. J. Verbiscer, H. A. Weaver,
 1248 and L. A. Young. Pluto’s global surface composition through pixel-by-pixel
 1249 Hapke modeling of New Horizons Ralph/LEISA data. *Icarus*, 287:218–228,
 1250 May 2017. doi: 10.1016/j.icarus.2016.11.028.
- 1251 G. Robuchon and F. Nimmo. Thermal evolution of Pluto and implications for

- 1252 surface tectonics and a subsurface ocean. *Icarus*, 216:426–439, December
 1253 2011. doi: 10.1016/j.icarus.2011.08.015.
- 1254 P. Schenk, R. A. Beyer, J. M. Moore, J. R. Spencer, W. B. McKinnon, H. A.
 1255 Weaver, Jr., L. A. Young, C. Olkin, K. Ennico Smith, and A. Stern. Regional
 1256 Topographic Properties of Pluto and Charon from New Horizons. *AGU Fall*
 1257 *Meeting Abstracts*, February 2016a.
- 1258 P. Schenk, K. Singer, S. Robbins, V. Bray, R. Beyer, J. Moore, W. B. McKin-
 1259 non, J. Spencer, K. Runyon, S. A. Stern, L. A. Young, C. Olkin, K. Ennico,
 1260 and H. A. Weaver. Topography of Pluto and Charon: Impact Cratering. In
 1261 *Lunar and Planetary Science Conference*, volume 47 of *Lunar and Planetary*
 1262 *Science Conference*, page 2795, March 2016b.
- 1263 P. Schenk, R. A. Beyer, W. B. McKinnon, J. M. Moore, J. R. Spencer, O. M.
 1264 White, K. Singer, S. Robbins, O. M. Umurhan, F. Nimmo, T. D. Lauer,
 1265 W. Grundy, A. Stern, H. A. Weaver, Jr., L. A. Young, C. Olkin, the New
 1266 Horizons Geology, and Geophysics Investigation Team. Basins, Fractures
 1267 and Volcanoes: Global Cartography and Topography of Pluto from New
 1268 Horizons. *Submitted to Icarus*, August 2018a.
- 1269 P. Schenk, R. A. Beyer, J. M. Moore, J. R. Spencer, W. B. McKinnon, H. A.
 1270 Weaver, Jr., L. A. Young, C. Olkin, K. Ennico Smith, and A. Stern. To-
 1271 pography of Sputnik Planitia Basin on Pluto: What We Know and Don’t
 1272 Know. *AGU Fall Meeting Abstracts*, February 2018b.
- 1273 B. Schmitt, S. Philippe, W. M. Grundy, D. C. Reuter, R. Cote, E. Quirico,
 1274 S. Protopapa, L. A. Young, R. P. Binzel, J. C. Cook, D. P. Cruikshank, C. M.
 1275 Dalle Ore, A. M. Earle, K. Ennico, C. J. A. Howett, D. E. Jennings, I. R.
 1276 Linscott, A. W. Lunsford, C. B. Olkin, A. H. Parker, J. W. Parker, K. N.
 1277 Singer, J. R. Spencer, J. A. Stansberry, S. A. Stern, C. C. C. Tsang, A. J.
 1278 Verbiscer, and H. A. Weaver. Physical state and distribution of materials
 1279 at the surface of Pluto from New Horizons LEISA imaging spectrometer.
 1280 *Icarus*, 287:229–260, May 2017. doi: 10.1016/j.icarus.2016.12.025.
- 1281 T. Schneider, S. D. B. Graves, E. L. Schaller, and M. E. Brown. Polar methane
 1282 accumulation and rainstorms on Titan from simulations of the methane
 1283 cycle. *Nature*, 481:58–61, January 2012. doi: 10.1038/nature10666.
- 1284 T. A. Scott. Solid and liquid nitrogen. *Phys. Rep.*, 27:89–157, September
 1285 1976. doi: 10.1016/0370-1573(76)90032-6.
- 1286 S. A. Stern, F. Bagenal, K. Ennico, G. R. Gladstone, W. M. Grundy, W. B.
 1287 McKinnon, J. M. Moore, C. B. Olkin, J. R. Spencer, H. A. Weaver, L. A.
 1288 Young, T. Andert, J. Andrews, M. Banks, B. Bauer, J. Bauman, O. S.
 1289 Barnouin, P. Bedini, K. Beisser, R. A. Beyer, S. Bhaskaran, R. P. Binzel,
 1290 E. Birath, M. Bird, D. J. Bogan, A. Bowman, V. J. Bray, M. Brozovic,
 1291 C. Bryan, M. R. Buckley, M. W. Buie, B. J. Buratti, S. S. Bushman, A. Cal-
 1292 loway, B. Carcich, A. F. Cheng, S. Conard, C. A. Conrad, J. C. Cook, D. P.
 1293 Cruikshank, O. S. Custodio, C. M. Dalle Ore, C. Deboy, Z. J. B. Dischner,
 1294 P. Dumont, A. M. Earle, H. A. Elliott, J. Ercol, C. M. Ernst, T. Finley, S. H.
 1295 Flanigan, G. Fountain, M. J. Freeze, T. Greathouse, J. L. Green, Y. Guo,
 1296 M. Hahn, D. P. Hamilton, S. A. Hamilton, J. Hanley, A. Harch, H. M.

- 1297 Hart, C. B. Hersman, A. Hill, M. E. Hill, D. P. Hinson, M. E. Holdridge,
1298 M. Horanyi, A. D. Howard, C. J. A. Howett, C. Jackman, R. A. Jacobson,
1299 D. E. Jennings, J. A. Kammer, H. K. Kang, D. E. Kaufmann, P. Koll-
1300 mann, S. M. Krimigis, D. Kusnierkiewicz, T. R. Lauer, J. E. Lee, K. L.
1301 Lindstrom, I. R. Linscott, C. M. Lisse, A. W. Lunsford, V. A. Mallder,
1302 N. Martin, D. J. McComas, R. L. McNutt, D. Mehoke, T. Mehoke, E. D.
1303 Melin, M. Mutchler, D. Nelson, F. Nimmo, J. I. Nunez, A. Ocampo, W. M.
1304 Owen, M. Paetzold, B. Page, A. H. Parker, J. W. Parker, F. Pelletier, J. Pe-
1305 terson, N. Pinkine, M. Piquette, S. B. Porter, S. Protopapa, J. Redfern, H. J.
1306 Reitsema, D. C. Reuter, J. H. Roberts, S. J. Robbins, G. Rogers, D. Rose,
1307 K. Runyon, K. D. Retherford, M. G. Ryschkewitsch, P. Schenk, E. Schind-
1308 helm, B. Sepan, M. R. Showalter, K. N. Singer, M. Soluri, D. Stanbridge,
1309 A. J. Steffl, D. F. Strobel, T. Stryk, M. E. Summers, J. R. Szalay, M. Ta-
1310 pley, A. Taylor, H. Taylor, H. B. Throop, C. C. C. Tsang, G. L. Tyler,
1311 O. M. Umurhan, A. J. Verbiscer, M. H. Versteeg, M. Vincent, R. Webbert,
1312 S. Weidner, G. E. Weigle, O. L. White, K. Whittenburg, B. G. Williams,
1313 K. Williams, S. Williams, W. W. Woods, A. M. Zangari, and E. Zirnstein.
1314 The Pluto system: Initial results from its exploration by New Horizons.
1315 *Science*, 350:aad1815, October 2015. doi: 10.1126/science.aad1815.
- 1316 S. A. Stern, R. P. Binzel, A. M. Earle, K. N. Singer, L. A. Young, H. A.
1317 Weaver, C. B. Olkin, K. Ennico, J. M. Moore, W. B. McKinnon, and J. R.
1318 Spencer. Past epochs of significantly higher pressure atmospheres on Pluto.
1319 *Icarus*, 287:47–53, May 2017. doi: 10.1016/j.icarus.2016.11.022.
- 1320 A. J. Trowbridge, H. J. Melosh, J. K. Steckloff, and A. M. Freed. Vigorous
1321 convection as the explanation for Pluto’s polygonal terrain. *Nature*, 534:
1322 79–81, June 2016. doi: 10.1038/nature18016.
- 1323 O. M. Umurhan, A. D. Howard, J. M. Moore, A. M. Earle, O. L. White, P. M.
1324 Schenk, R. P. Binzel, S. A. Stern, R. A. Beyer, F. Nimmo, W. B. McKinnon,
1325 K. Ennico, C. B. Olkin, H. A. Weaver, and L. A. Young. Modeling glacial
1326 flow on and onto Pluto’s Sputnik Planitia. *Icarus*, 287:301–319, May 2017.
1327 doi: 10.1016/j.icarus.2017.01.017.
- 1328 O. L. White, J. M. Moore, W. B. McKinnon, J. R. Spencer, A. D. Howard,
1329 P. M. Schenk, R. A. Beyer, F. Nimmo, K. N. Singer, O. M. Umurhan,
1330 S. A. Stern, K. Ennico, C. B. Olkin, H. A. Weaver, L. A. Young, A. F.
1331 Cheng, T. Bertrand, R. P. Binzel, A. M. Earle, W. M. Grundy, T. R. Lauer,
1332 S. Protopapa, S. J. Robbins, and B. Schmitt. Geological mapping of Sputnik
1333 Planitia on Pluto. *Icarus*, 287:261–286, May 2017. doi: 10.1016/j.icarus.
1334 2017.01.011.
- 1335 R. Wordsworth, F. Forget, E. Millour, J. W. Head, J.-B. Madeleine, and
1336 B. Charnay. Global modelling of the early martian climate under a denser
1337 CO₂ atmosphere: Water cycle and ice evolution. *Icarus*, 222:1–19, January
1338 2013. doi: 10.1016/j.icarus.2012.09.036.
- 1339 Y. Yamashita, M. Kato, and M. Arakawa. Experimental study on the rhe-
1340 ological properties of polycrystalline solid nitrogen and methane: Implica-
1341 tions for tectonic processes on Triton. *Icarus*, 207:972–977, June 2010. doi:

1342 10.1016/j.icarus.2009.11.032.
1343 A. Zangari. A meta-analysis of coordinate systems and bibliography of their
1344 use on Pluto from Charon's discovery to the present day. *Icarus*, 246:93–145,
1345 January 2015. doi: 10.1016/j.icarus.2014.10.040.

1346 **Acknowledgements**

1347 We acknowledge the Centre National d'Etudes Spatiales (CNES) for its finan-
1348 cial support through its "Système Solaire" program. The authors thank the
1349 whole NASA *New Horizons* instrument and scientific team for their excellent
1350 work on a fantastic mission and their interest in this research.